

國立台灣大學理學院地質科學所



碩士論文

Department of Geosciences

College of Science

National Taiwan University

Master Thesis

一萬六千五百年來東帝汶降雨變遷

Precipitation variability in East Timor during the Last
16,500 years

陳晉平

Jin-Ping Chen

指導教授：沈川洲 博士

Advisor: Chuan-Chou Shen, Ph. D.

中華民國 102 年 8 月

August, 2013

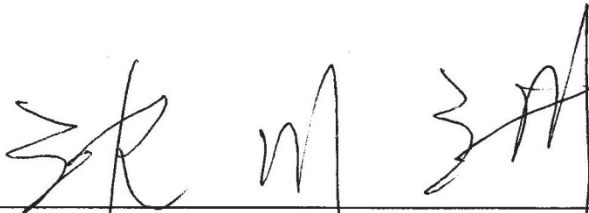
國立臺灣大學碩士學位論文
口試委員會審定書

一萬六千五百年來東帝汶降雨變遷

Precipitation variability in East Timor during the last
16,500 years

本論文係陳晉平君（學號 R00224110）在國立臺灣大學地質科學所完成之碩士學位論文，於民國 102 年 7 月 25 日承下列考試委員審查通過及口試及格，特此證明

口試委員：



(指導教授) (簽名)

李時雨

朱所生

魏國亨

誌謝



能夠順利取得這個學位，要感謝的人太多了。首先是我的**指導老師沈川洲教授**，除了要感謝老師的悉心指導與支持，以及充滿耐心的論文、海報修改，沈老師對於分析化學的精確與學術熱忱也帶給我許多啟發。並感謝**魏國彥教授**、**米泓生教授**以及**李時兩老師**等各位口試委員，給予的建議與指教。魏老師所的古生物學，以及其他課堂、會議中的討論，賦予我對於古氣候、古環境更深一層的認識；**羅立學長**以及**林蔭學長**給了我們這些傻蛋許多有用的提示和指引，真是數也數不清。感謝**林可學姊**帶我入門鈾鈦定年和實驗室總總細節的入門，感謝**吳忠哲學長**與**姜修洋老師**與幫我們排解了許多儀器的疑難雜症。感謝米老師和九州大學的**狩野彰宏教授**慷慨提供碳氧同位素測定設備，並感謝**楊琇玉學姊**、**劉文琳學姊**以及**曾根知實小姐**幫我測定了大量樣本。感謝**陳怡綺學姊**和**黃莉容學姊**的論文，以及**周瑜蓁學姊**和**張育維學長**的幫助。也謝謝我的同學**皓正兄**和**建儒兄**，還有我的家人的扶持，讓我撐到畢業。

修讀碩士班的所獲得的體驗，其價值對我來說遠超過文憑本身；我能夠說，在我受完地質系碩士班的訓練後，不僅對於地質與學術有了更深一層認識，也成為了一個更好的人。

Abstract



Here we present replicated stalagmite analysis $\delta^{18}\text{O}$ records over the past 16.5 thousand years (ka, before 1950 AD) with a gap of 11.5-5.7 ka of three stalagmites from Lekiraka cave in East Timor ($8^{\circ}47'10.8''\text{S}$, $126^{\circ}23'31.1''\text{E}$; 626 m above sea level). Lekiraka $\delta^{18}\text{O}$ record suggests a relatively dry condition during the glacial period, comparing with the late Holocene. Depletion in ^{18}O during Younger Dryas (YD) stadial suggests a wet condition with high precipitation, which is consistent with that of Liang Luar cave record in Flores, but in contrary to a dry condition in the Asian monsoon (AM) territory. Insignificant $\delta^{18}\text{O}$ change during 16-12 ka indicates that a wet Bølling-Allerød (BA) interstadial in AM territory is not clear at this low-latitude zone. We propose that the intensified precipitation in YD and “muted” BA could be attributed to: (1) enhanced Australian-Indonesian summer monsoon (AISM), (2) displacement of Intertropical Convergence Zone (ITCZ), and/or (3) exposed Sunda shelf landmass lead to change of the regional atmospheric circulation.

摘要



本研究利用取自東帝汶猴洞(南緯八度四十七分十點八秒，東經一百二十六度二十三分三十一點一秒，海拔六百二十六公尺)之三株石筍，重建並分析 16.5 千年前(ka, before 1950AD)以來之區域古水文變遷(於 11.5 至 5.7 千年具年代間斷)。具重現性之東帝汶石筍之穩定氧同位素($\delta^{18}\text{O}$)時間序列顯示，相對於中晚全新世，該區域之氣候於末次冰期處於相對乾燥之狀況。本紀錄於新仙女木期(Younger Dryas, YD)時間段之石筍 ^{18}O 相對匱乏，顯示該時期為相對潮濕、高降雨之氣候狀況，與鄰近區域前人研究結果一致(Liang Luar cave, Flores)，並與典型亞洲季風(Asian Monsoon, AM)區域古氣候紀錄於該時期所呈現之相對乾燥、低降雨狀況，呈反向對應。本紀錄中，16 千年至 12 千年間之千年尺度氣候事件波動並不似典型亞洲季風區所顯示之明顯與強烈，Bølling-Allerød (B-A)暖期亦未有明顯暖化跡象，猜測可能原因為：(一)，印澳夏季季風(Australian-Indonesian summer monsoon, AISM)之增強；(二)，間熱帶輻合區(Intertropical Convergence Zone, ITCZ)之位移；以及/或(三)，巽他陸棚(Sunda Shelf)出露所導致之區域水氣循環變遷。

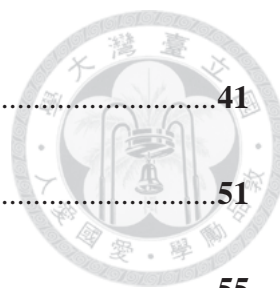
Content



Abstract	I
摘要	II
Content	III
List of Figures	V
List of Tables	VI
Chapter 1 Introduction	1
1.1 Inter-hemispheric anti-phasing behavior of millennium-scale climate events	1
1.2 Indo-Pacific warm pool	2
1.3 Australian-Indonesian monsoon	4
Chapter 2 Regional setting and methods	6
2.1 Study site and research material	6
2.1.1 Location of Lekiraka cave.....	6
2.1.2 Regional settings	8
2.2 Experiments	9
2.2.1 Subsampling.....	9



2.2.2 Labwares for U-Th dating chemical procedure	9
2.2.3 U-Th dating chemical procedure.....	9
2.2.4 U-Th dating Instrumentation.....	12
2.2.5 Stable oxygen isotope analysis Instrumentation	13
2.2.6 Hendy Test and Replication Test	14
Chapter 3 Results	15
3.1 U-Th dating results and age model	15
3.2 Oxygen and carbon stable isotope records.....	22
3.2.1 Hendy Test and Replication Test	22
3.2.2 Oxygen stable isotope time series	24
Chapter 4 Discussion	26
4.1 Fluctuation of hydroclimate in Australian-Indonesian monsoon territory since the last 16,500 years.....	26
4.2 Comparison with global and regional paleoclimate proxy records	33
4.2.1 Late Pleistocene --- From H1 to YD	33
4.2.2 Middle to Late Holocene.....	38
Chapter 5 Conclusions	40



References	41
Appendix (I) U-Th concentration data and dating results	51
Appendix (II) $\delta^{18}\text{O}$ records	55

List of Figures

Figure 1-1. Reconstructed SST of equatorial Pacific sediment cores	3
Figure 1-2. Main atmospheric features in the modern western Pacific	5
Figure 2-1. Map with cave and marine sediment core locations	6
Figure 2-2. Stalagmite samples, from the cave to the laboratory	7
Figure 2-3. Average rainfall amount / temperature of Ossu	8
Figure 3-1. Plot of sample depth versus age for three selected stalagmites	16
Figure 3-2. Stalagmite MC110803-1	18
Figure 3-3. Stalagmite MC110803-2	20
Figure 3-4. Stalagmite 090721-2MC	21
Figure 3-5. Results of ‘Hendy Test’ of Lekiraka stalagmites	23
Figure 3-6. $\delta^{18}\text{O}$ records of Lekiraka stalagmites	25
Figure 4-1. Map with site locations and moisture trajectories	27
Figure 4-2. Moisture trajectories for Laing Luar cave	28
Figure 4-3. Map with site locations and seasonal climate information	29



Figure 4-4. Present-day IPWP hydroclimate	30
Figure 4-5. Paleoclimate proxy records over the past 18,000 years.....	32
Figure 4-6. Simulation result of the global general circulation model.....	34
Figure 4-7. Reconstruction of Sunda shelf sea-level during at 12.31 ka BP.....	36
Figure 4-8. Simulated Indo-Pacific Walker circulation change in the LGM.....	37
Figure 4-9. Simulated LGM changes in the Indo-Pacific.....	37
Figure 4-10. Paleoclimate proxy records over the past 6,000 years.....	39

List of Tables


Table 3-1. ^{230}Th age data of stalagmite MC110803-1	17
Table 3-2. ^{230}Th age data of stalagmite MC110803-2.....	19
Table 3-3. ^{230}Th age data of stalagmite 090721-2MC.....	21

Chapter 1 Introduction



1.1 Inter-hemispheric anti-phasing behavior of millennium-scale climate events

High-resolution paleoclimate proxy records during the last glacial period have been reported over past decades using different natural archives, such as ice cores (North Greenland Ice Core Project members, 2004; Petit *et al.*, 1999; Stenni *et al.*, 2011), stalagmites (Cruz *et al.*, 2006; Dykoski *et al.*, 2005; Fleitmann *et al.*, 2004; Wang *et al.*, 2001; Wang *et al.*, 2006), and marine foraminifera (Kiefer and Kienast, 2005; Mohtadi *et al.*, 2011; Xu *et al.*, 2010). The anti-phasing variation between millennium-scale climate changes at Heinrich event 1 (H1) stadial, Younger Dryas (YD) stadial, and Bølling-Allerød (BA) interstadial during the last glacial-interglacial period over the Northern Hemisphere (NH) and the Southern Hemisphere (SH) was revealed (Fig. 1-1) (Barker *et al.*, 2009). The phenomenon was suggested to be contributed to fluctuation of high-latitude Atlantic meridional overturning circulation (AMOC), induced by rapid fresh water discharge (Denton *et al.*, 2010; McManus *et al.*, 2004; Stenni *et al.*, 2011). However, AMOC reduction events and these millennium-scale climate events in low-latitude proxy records are rather subtle since the last glacial maximum (LGM), and only few terrestrial paleoclimate high-resolution proxy records were available at the low-latitude zones (Cruz *et al.*, 2009; Griffiths *et al.*, 2009; Partin *et al.*, 2007; Wang *et*



al., 2006). Therefore, in order to clarify the teleconnection between North Atlantic dynamic and low-latitude atmospheric perturbation, further insight to past activity of Pacific side low-latitude major climate system such as the Indo-Pacific warm pool (IPWP) and the Australian-Indonesian monsoon (AIM), is crucial for deciphering global climate change.

1.2 Indo-Pacific warm pool

Many marine sediment cores obtained from the IPWP had been studied (Kiefer and Kienast, 2005; Visser, Thunell and Stott 2003; Xu *et al.*, 2010). The paleoclimate proxy records suggest a substantially different regional climate development, comparing to those of the high-latitude NH. Instead of profound signature of millennial climate events, most of the IPWP proxy records show a constant warming situation since the LGM (Kiefer and Kienast, 2005; Rosenthal *et al.*, 2003; Stott, 2002).

Previous studies indicate that the IPWP does not only act as a fundamental role in the climate system of South-East Asia, but also be likely important for propagation and amplification of millennial climate events (Abram *et al.*, 2009; DiNezio *et al.*, 2013; Tokinaga *et al.*, 2012).

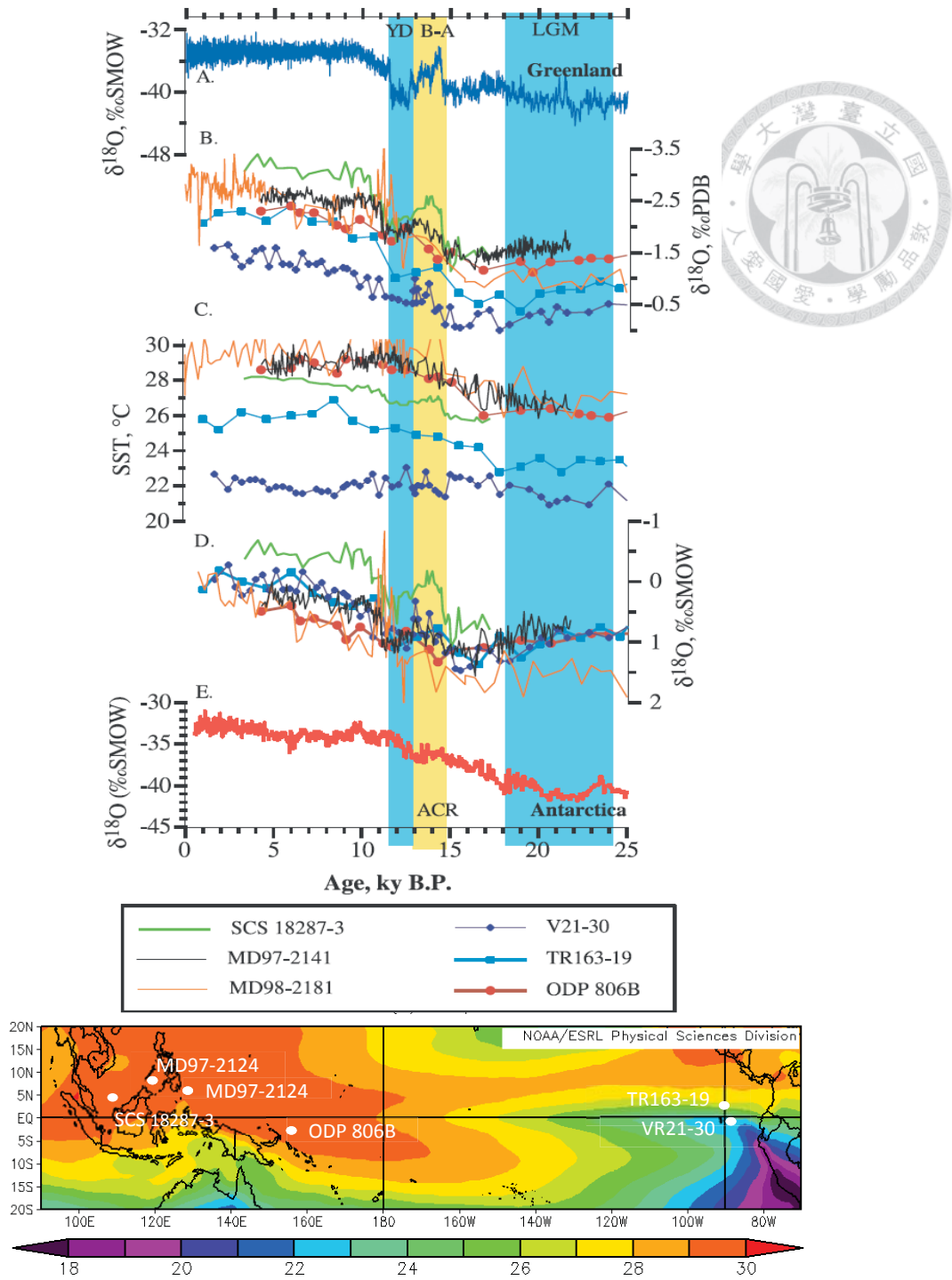


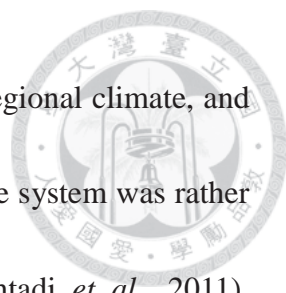
Figure 1-1. Reconstructed SSTs of equatorial Pacific sediment cores compared with ice core $\delta^{18}\text{O}$ records. Comparison of equatorial Pacific Ocean sediment core records (modified from Rosenthal *et al.*, 2003). (A) NGRIP ice core $\delta^{18}\text{O}$ record from Greenland (North Greenland Ice Core Project members, 2004). Planktonic foraminiferal derived (B) $\delta^{18}\text{O}$ and (C) SST record. (D) Surface sea water $\delta^{18}\text{O}$ record. (E) Byrd ice core $\delta^{18}\text{O}$ record from Antarctica (Blunier and Brook, 2001).



1.3 Australian-Indonesian monsoon

Dynamics of AIM, bearing strong connection with East Asian Monsoon (EAM) system (Fig. 1-2), since the last glacial are rather less studied. Paleoclimate model experiments (Wyrwoll *et al.*, 2007), paleoproductivity data (Holbourn *et al.*, 2005) and pollen records (Kershaw, van der Kaars and Moss 2003) revealed that variation of SH summer insolation influence Australian-Indonesian summer monsoon (AISM) rainfall on orbital timescale. In contrast, Miller *et al.* (2005) suggested that the dominant AISM forcing is the strength of the East Asian winter monsoon (Miller *et al.*, 2005), which is governed by the strength of air outflowing from the semi-permanent high-pressure system over Siberia. During the Holocene epoch, the mechanisms that drive millennial- and centennial- scale events is poorly known. The current available coral records (Abram *et al.*, 2007; Tudhope *et al.*, 2001) and ocean sediment core records (Stott *et al.*, 2004; Visser, Thunell and Stott 2003) only provide limited information. Model experiments simulated perturbation of regional atmospheric circulation and millennial-scale events since the LGM (DiNezio *et al.*, 2013; Tokinaga *et al.*, 2012; Zhang and Delworth, 2005), revealing significant influence of Sunda Shelf exposure on AIM dynamics.

Previous studies have suggested that (1) the AIM system was dominated by insolation intensity and/or sea-level on orbital time scale (Griffiths *et al.*, 2009; Miller *et*



al., 2005), (2) exposure of the Sunda Shelf may profoundly affect regional climate, and (DiNezio *et al.*, 2013; Tokinaga *et al.*, 2012) and (3) regional climate system was rather heterogeneous than previous thought (DiNezio *et al.*, 2013; Mohtadi *et al.*, 2011). Located at the modern southern border of Austral winter ITCZ, hydroclimate condition of East Timor is dominantly affected by AM and AIM dynamics (An *et al.*, 2000; Griffiths *et al.*, 2009). Therefore, by acquiring high-resolution proxy records from East Timor stalagmites, our goal is to clarify how the AIM system responds to regional and global changes, and have further insight on teleconnection between North Atlantic perturbation and low-latitude climate system since the LGM.

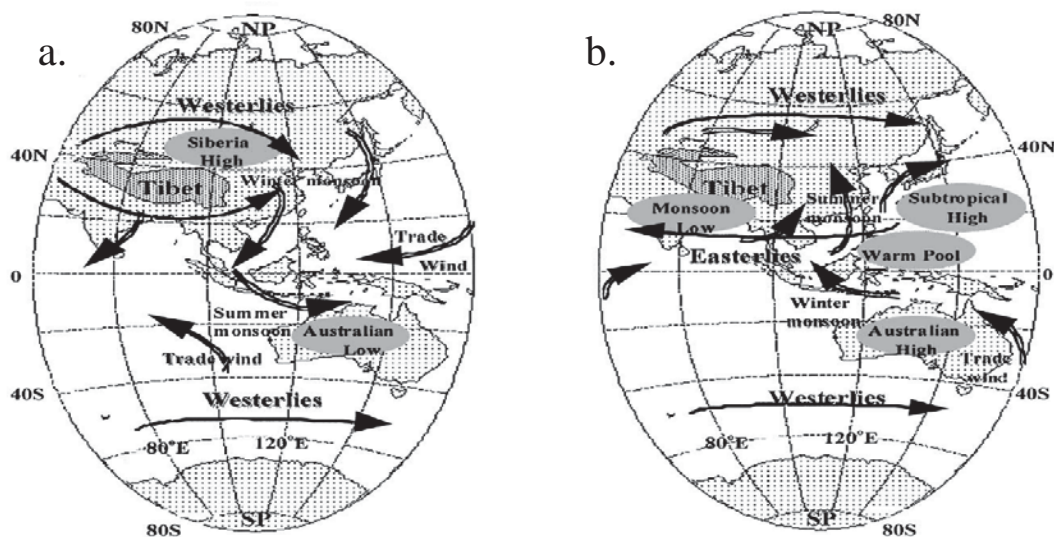


Figure 1-2. Main atmospheric features in the modern western Pacific. Schematic view of major atmospheric system during austral winter (June to August) (a) and austral summer (December to February) (b). The dominant flows in the middle and low troposphere are indicated by closed and open arrows, respectively (An *et al.*, 2000).

Chapter 2 Regional settings and methods



2.1 Study site and research material

2.1.1 Location of Lekiraka cave

Stalagmites were obtained from Lekiraka cave, Ossu, Viqueque, East Timor (Fig 2-2). This cave is located at $8^{\circ}47'10.8''\text{S}$, $126^{\circ}23'31.1''\text{E}$; 626 m above sea level, with limestone cap layer about 20m. Lekiraka cave is about 650 km east to the Liang Luar cave (Flores, Indonesia, $8^{\circ}32'\text{S}$, $120^{\circ}26'\text{E}$; 550 m above sea level) (Griffiths *et al.*, 2009).

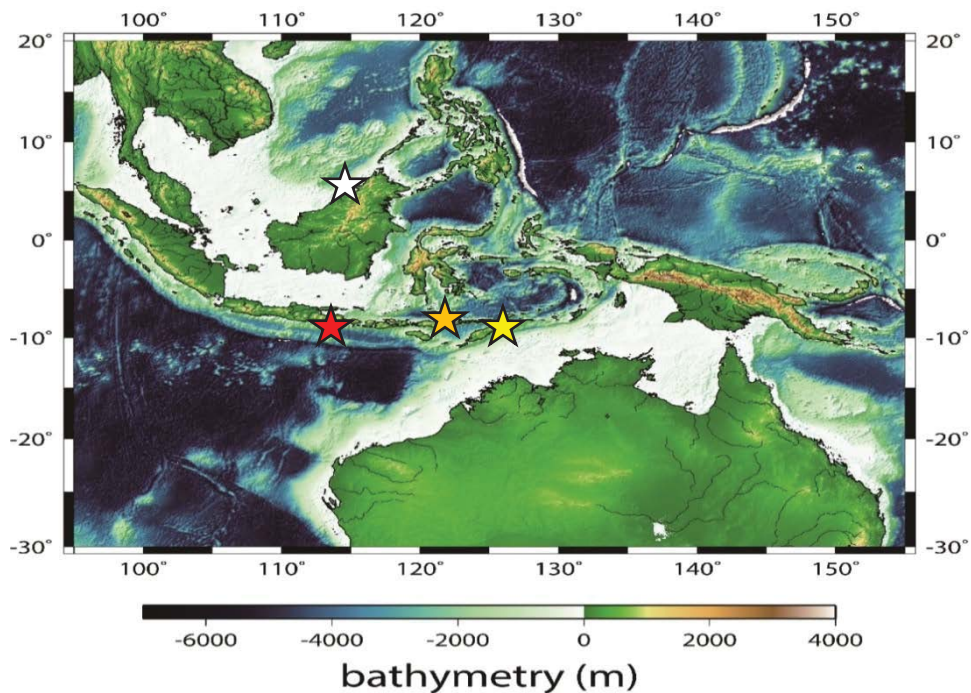


Figure 2-1. Map showing cave and marine sediment core locations. Stars denote the locations of Lekiraka cave (yellow), Liang Luar cave (orange) (Griffiths *et al.*, 2009), Gunung Buda (white) (Partin *et al.*, 2007), and sediment core GeoB10053-7 (red) (Mohtadi *et al.*, 2011).

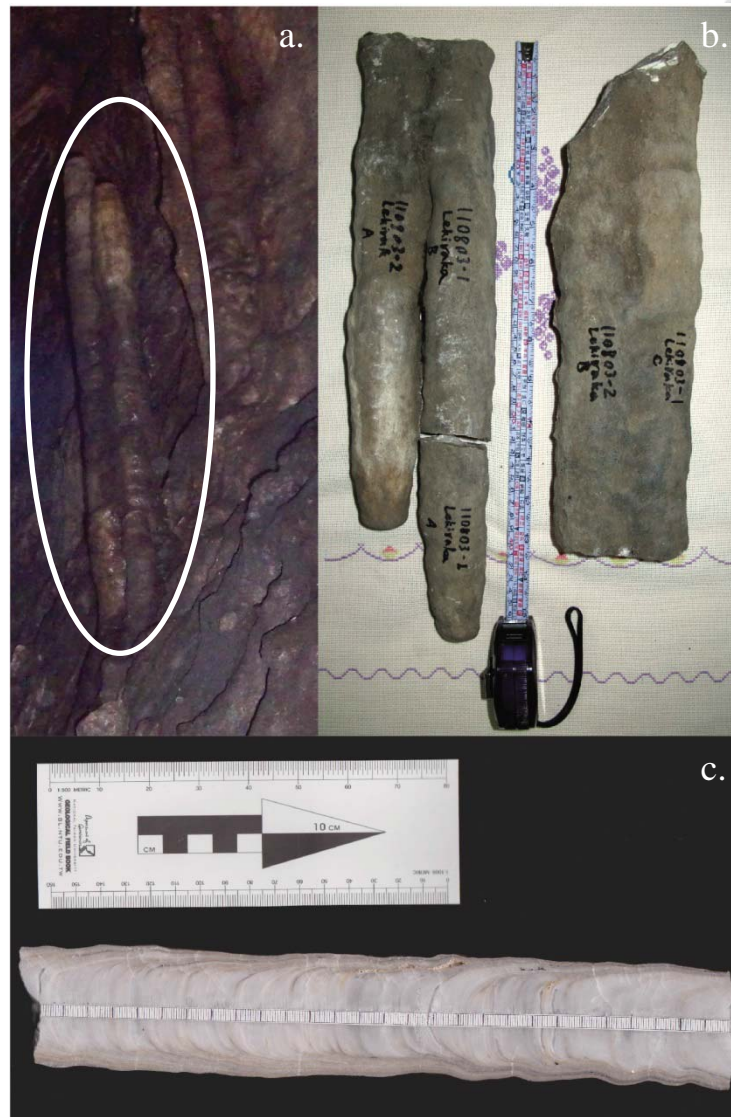


Figure 2-2. Stalagmite samples, from the cave to the laboratory. (a) Stalagmites in the Lekiraka cave, highlighted by white circle. (b) Unprocessed stalagmite samples. (c) Stalagmite samples that were halved, polished, ready for subsampling.



2.1.2 Regional settings

The air temperature of Lekiraka cave is 25.3°C, with relative humidity of 97% (August 3rd, 2011). The annual mean temperature of Ossu, the cave site is 26.1°C, with mean annual rainfall of 1948 mm recorded by the Ossu weather station, for ~57% falling during austral summer monsoon season (December–March) and ~17% falling during austral winter monsoon season (June–September) (Fig. 2-3).

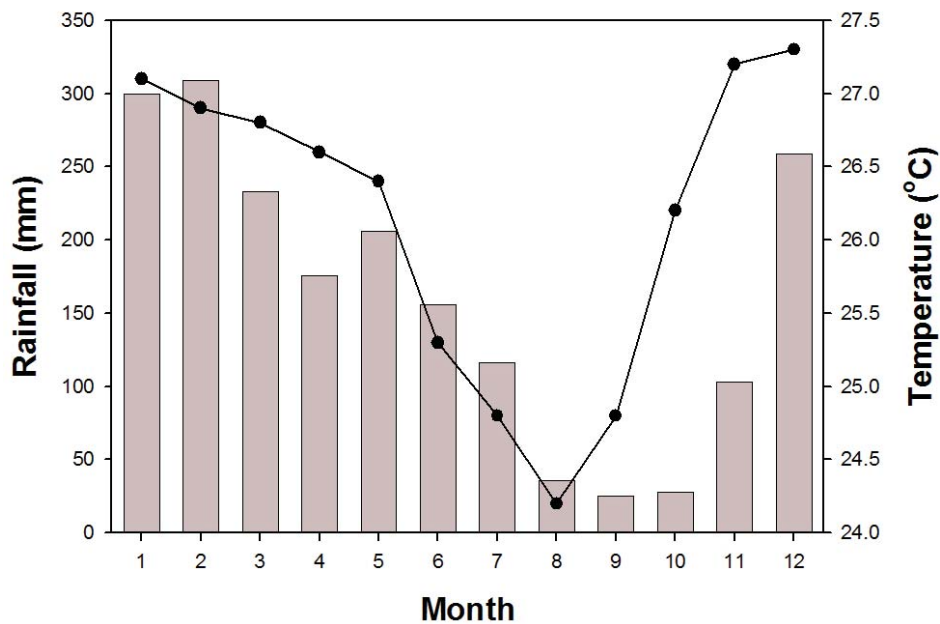


Figure 2-3. Average rainfall amount / temperature of Ossu. Long-term (1952-1974 AD) monthly average rainfall amount (grey bars) and temperature (black circles) of Ossu weather station. Data was obtained from Timor-Leste Meteorology Center.



2.2 Experiments

2.2.1 Subsampling

Stalagmite were halved and polished. For U-Th dating, powdered samples, 50-120 mg each, were milled along the growth layer. For stable oxygen and carbon isotope time series, powder samples, 50-100 μg each, were milled along the growth axis. For 'Hendy Test' (Hendy *et al.*, 1971), powdered samples, 50-100 μg each, were milled along the coeval growth layers with interval of 1 mm. All sub-sampling procedure was performed in class-10000 sub-sampling room and class-100 benches.

2.2.2 Labwares for U-Th dating chemical procedure

Labware used in this research included Teflon beakers, bottles, and columns; PE/PP bottles, centrifuge tubes, vials, pipette tips, and porous PP column frits. In order to reduce chemical blank during U-Th isotope measurement, all labwares were acid-cleaned (Shen *et al.*, 2003) prior to U-Th dating chemical procedure (Shen *et al.*, 2003; Shen *et al.*, 2012).

2.2.3 U-Th dating chemical procedure

For reduction of potential containment, the chemical procedure for U-Th dating was performed in a class-10,000 clean room with independent class-100 benches and hoods. U-Th dating chemical procedure was developed in HISPEC, Department of Geosciences, National Taiwan University (Shen *et al.*, 2003).



Sample digestion

1. Stalagmite powdered sample was weighed and preserved in a 30-ml Teflon beaker.
2. Sample was covered with pure water, and dissolved gradually by adding appropriate drops of 14N HNO₃.
3. Appropriate amount of ²²⁹Th-²³³U-²³⁶U spike solution was added and weighed.
4. Ten drops of HClO₄ were added for removal of organic matters.
5. One drop of FeCl₂ was added for iron co-precipitation.
6. The sample solution was refluxed at 200°C on a hotplate over 12 hours to achieve complete U-Th isotopic equilibrium and decomposition of organic matters.
7. The sample solution was dried at 250 °C.

Iron co-precipitation and centrifugation

1. Dehydrated sample was covered with 1-2 ml pure H₂O, and dissolved with 1-2 ml 2 N HCl, then transferred from Teflon beaker into a PE centrifuge tube. The Teflon beaker was cleaned with dilute aqua regia.
2. Appropriate amount of NH₄OH was gradually added to the sample solution, until Fe(OH)₃ precipitate (for uranium and thorium co-precipitation).
3. Suspension was then separated by centrifugation and discarded, and residual was rinsed by appropriate amount of pure H₂O. This step was repeated three times.
4. Ten drops of 14 N HNO₃ were added to dissolve the residual, and transferred back

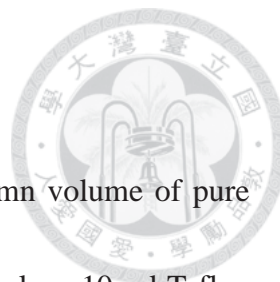


into the original Teflon beaker.

5. Two drops of HClO_4 were added to the sample solution and dried at 250°C .
6. One drop of 14 N HNO_3 was added to dissolve the dehydrated sample, and then dried at 250°C . This step was repeated for three times, to keep cations in nitric form.
7. Dehydrated sample was dissolved with 4-5 ml 7 N HNO_3 .

Uranium and thorium extraction by anion-exchange resin column

1. A 6-7 cm long column was packed with AG 1-X8 anion-exchange resin was prepared.
2. One column volume of pure H_2O with one drop of 14 N HNO_3 was added to remove metal ion.
3. Repeatedly adding one drop of 7 N HNO_3 was added three times. One column volume of 7 N HNO_3 was then added to condition the column.
4. Sample solution was loaded into the column.
5. Repeatedly adding one drop of 7 N HNO_3 three times. One column volume of 7 N HNO_3 was then added to fully elute Fe^{3+} .
6. The Teflon beaker was refluxed with 15ml 1% aqua regia and 0.005 N HF for 10 minutes and then rinsed with pure H_2O .
7. Repeatedly adding one drop of 6 N HCl three times. One column volume of 6 N HCl was then added. The thorium fraction was collected with the original cleaned 30-ml Teflon beaker. Two drops of HClO_4 were added to the beaker to decompose organic



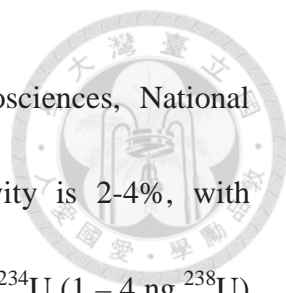
matters.

8. Repeatedly adding one drop of pure H₂O three times. One column volume of pure H₂O was then added. The uranium fraction was collected with a clean 10-ml Teflon beaker. Two drops of HClO₄ were added to the beaker to decompose organic matters.
9. The two separated thorium and uranium fraction were dried at 250 °C for fully dehydration.
10. One drop of HClO₄ was added to dissolve dehydrated sample. The sample was then dried at 250 °C to remove organic matter. This step was repeated for three times.
11. One drop of 14 N HNO₃ was added to dissolve dehydrated sample. The sample was dried at 250 °C. This step was repeated for three times.
12. The dried thorium and uranium fractions were dissolved with 1% aqua regia and 0.005 N HF and then transferred into PE vial from Teflon beaker for instrumental analysis.

2.2.4 U-Th dating Instrumentation

A Thermo-Fisher multiple-collector inductively coupled plasma mass spectrometer (MC-ICP-MS), equipped with a secondary electron multiplier (SEM) and combined with an Aridus sample introduction system was used for U-Th isotopic measurement.

U-Th dating techniques were developed in the High-Precision Mass Spectrometry and



Environment Change Laboratory (HISPEC), Department of Geosciences, National Taiwan University (Shen *et al.*, 2012). The instrument sensitivity is 2-4%, with precision of $\pm 1-2\%$ (2σ) for abundance determinations of 50-200 fg ^{234}U (1 – 4 ng ^{238}U) or ^{230}Th . One international standard, New Brunswick Laboratories Certified Reference Material 112A (NBL-112A) was used for calibrating mass fraction and intensity bias (Shen *et al.*, 2012).

2.2.5 Stable oxygen isotope analysis Instrumentation

Stable oxygen and carbon isotope analysis was performed in three laboratories. The first is the Kano Laboratory of the Department of Environmental Changes, Kyushu University. Isotopic measurement was conducted by Thermo-Finnigan Delta Plus mass spectrometer with GASBENCH II gas separation system. The second is Stable Isotope Laboratory of the Department of Earth Sciences, National Taiwan Normal University. Isotopic measurement was conducted by Micromass IsoPrime isotope ratio mass spectrometer (IRMS). The third is Stable Isotope Laboratory of the Department of Geoscience, National Taiwan University. Isotopic measurement was conducted by Thermo-Finnigan MAT 253 IRMS, with Kiel-II carbonate system. Oxygen and carbon stable isotopic data were reported as $\delta^{18}\text{O}$ and $\delta^{13}\text{C}$ respectively, relative to the Vienna Pee Dee Belemnite (VPDB) reference standard. The NBS-19 was used as calibration standard ($\delta^{18}\text{O} = -2.20\%$, $\delta^{13}\text{C} = +1.95\%$). One-sigma external precision of the

measurements was better than 0.08‰ for $\delta^{18}\text{O}$ and 0.04‰ for $\delta^{13}\text{C}$.



2.2.6 Hendy Test and Replication Test

‘Hendy Test’, a widely adapted testing method, was proposed by Hendy et. al. (1971), In order to preclude kinetic effect dominant stalagmites from providing biased paleoclimate proxy records. The Hendy test is based on two indicators that are established by the $\delta^{18}\text{O}$ and $\delta^{13}\text{C}$ value of subsamples in coeval stalagmite growth layers. First is the standard deviation of $\delta^{18}\text{O}$ value, and second is the covariation between $\delta^{18}\text{O}$ and $\delta^{13}\text{C}$ values. If $\delta^{18}\text{O}$ within the same layers have small σ value ($<0.5\%$) and/or $\delta^{18}\text{O}$ and $\delta^{13}\text{C}$ values are poorly correlated ($R^2 < 0.4$), the stalagmite is considered to precipitate without dominant kinetic fractionation, thus its $\delta^{18}\text{O}$ profile would be considered a valid paleoclimate proxy. Another relatively new and widely accepted testing method is ‘Replication Test’ (Dorale and Liu, 2004), by estimating the consistency between contemporaneous $\delta^{18}\text{O}$ profiles of stalagmites in different position of the cave. Dorale and Liu (2004) proposed that only when kinetic effect is absent or affect the stalagmites in the exact same way, will the different stalagmite $\delta^{18}\text{O}$ profiles be well duplicated, in which the latter case is fairly unlikely. This study adapted both approaches, to provide a robust examination.

Chapter 3 Results



3.1 U-Th dating results and age model

After screening, three stalagmites, MC110803-1, MC110803-2, and 090721-2MC were selected (Figs. 3-2 to 3-4). Age models of three selected stalagmite were constructed by 28 dating points, Age (before 1950 AD) intervals are 16.58-0.39 ka for MC110803-1, 14.62-0.87 ka for MC110803-2, and 13.16-11.62 ka for 090721-2MC (Fig. 3-1, Table 3-1 to 3-3). However, there is still a time gap at 11.6-5.7 ka in the spliced interval of 11.62 ka-5.64 ka. The average ^{238}U concentration of these three stalagmites is 285 ppb for MC110803-1, 266 ppb for MC110803-2, and 554 ppb for 090721-2MC, respectively. The detailed U-Th isotopic and concentration data and dating results are available in Appendix (I). The average growth rates of three stalagmites are 0.21, 0.092, and 0.056 mm/yr for MC110803-1, MC110803-2), and 090721-2MC, respectively.

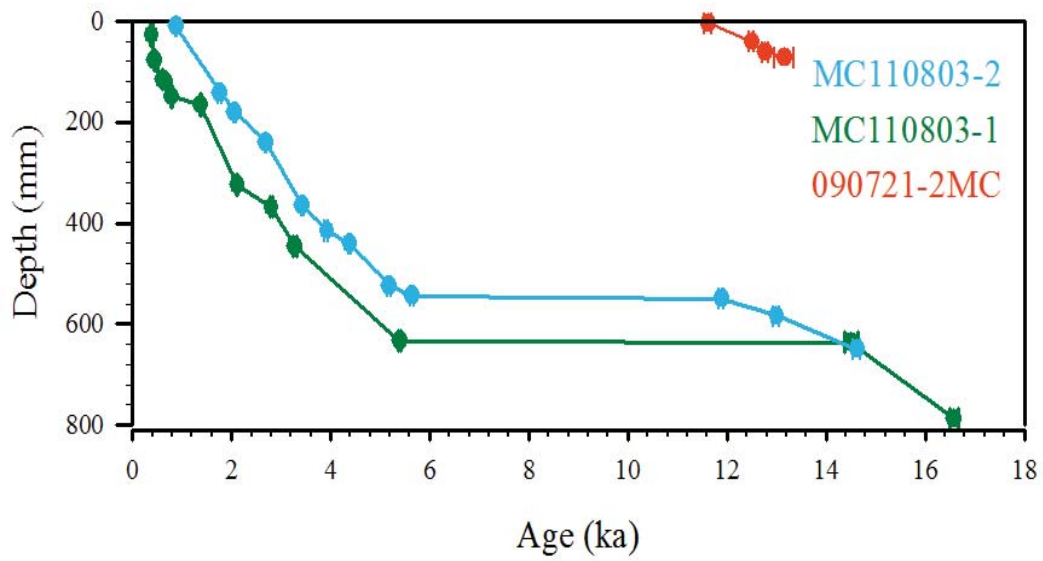


Figure 3-1. Plot of sample depth versus age for three selected Lekiraka cave stalagmites. Green, blue, and orange lines denote stalagmite MC110803-1, MC110803-2, and 090721-2MC, respectively. Most of 2σ error bars are smaller than the symbols.



Table 3-1. ^{230}Th age data of stalagmite MC110803-1.

Sample ID	Depth(mm)	Age (ka)	Error (2σ)
110803-1A-29	29	0.386	0.021
110803-1A-80	80	0.442	0.012
110803-1A-117	118	0.605	0.011
110803-1A-122	122	0.677	0.010
110803-1A-151	151	0.792	0.013
110803-1A-167	167	1.374	0.018
110803-1A-326.5	326.5	2.115	0.016
110803-1A-370.5	370.5	2.803	0.019
110803-1A-447.5	447.5	3.274	0.029
110803-1A-635.5	635.5	5.394	0.034
110803-1A-637.5	637.5	14.51	0.13
110803-1A-789	789	16.576	0.087

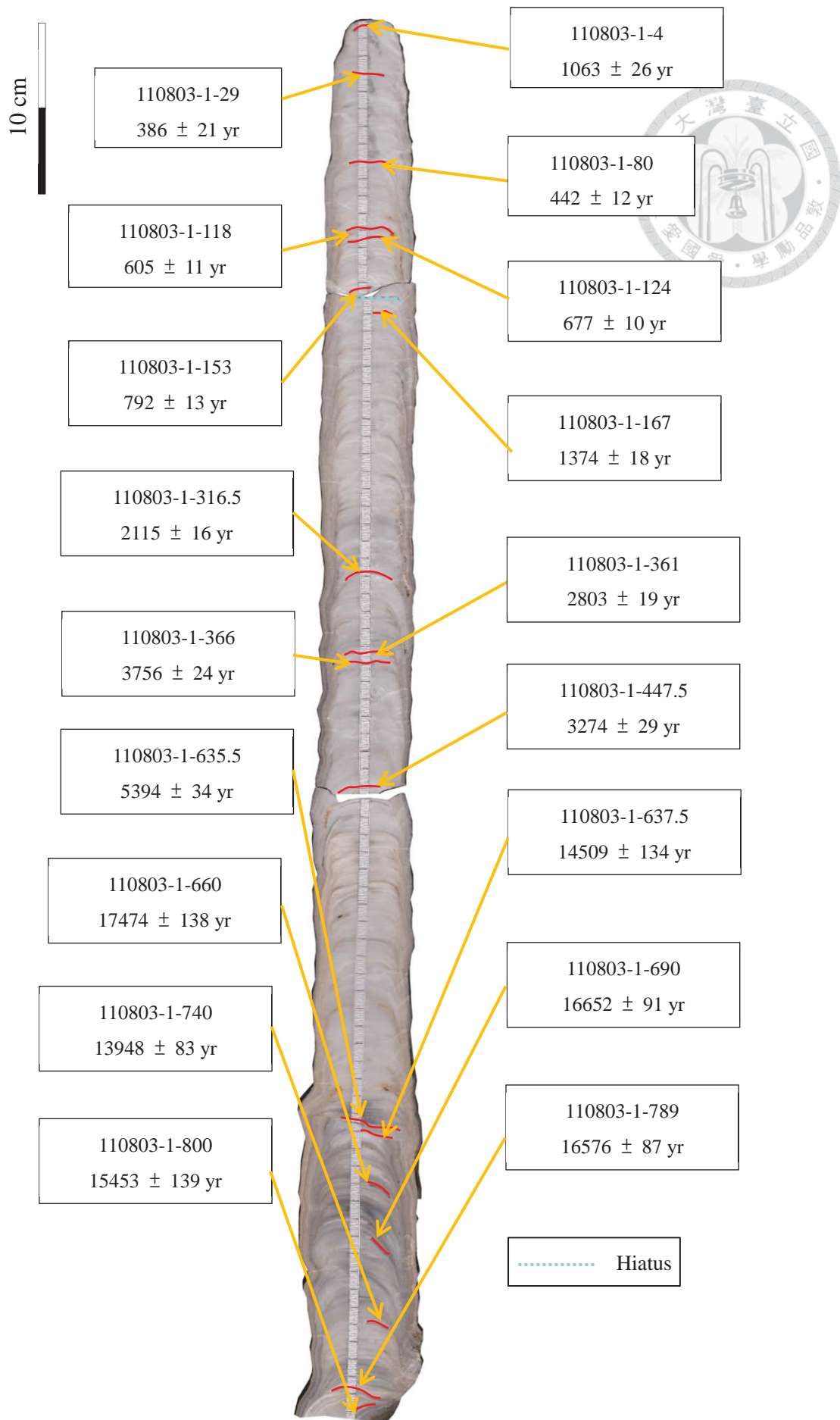


Figure 3-2. Stalagmite MC110803-1



Table 3-2. ^{230}Th age data of stalagmite MC110803-2.

Sample ID	Depth(mm)	Age (ka)	Error (2σ)
110803-2A-10	10	0.874	0.014
110803-2A-142	142	1.769	0.033
110803-2A-180	180	2.062	0.025
110803-2A-240	240	2.687	0.018
110803-2A-365	365	3.425	0.023
110803-2A-415	415	3.918	0.034
110803-2A-441	441	4.383	0.022
110803-2A-524	524	5.181	0.032
110803-2A-544	544	5.64	0.032
110803-2A-550	550	11.887	0.054
110803-2A-583.5	583.5	13.004	0.061
110803-2A-650	650	14.621	0.074

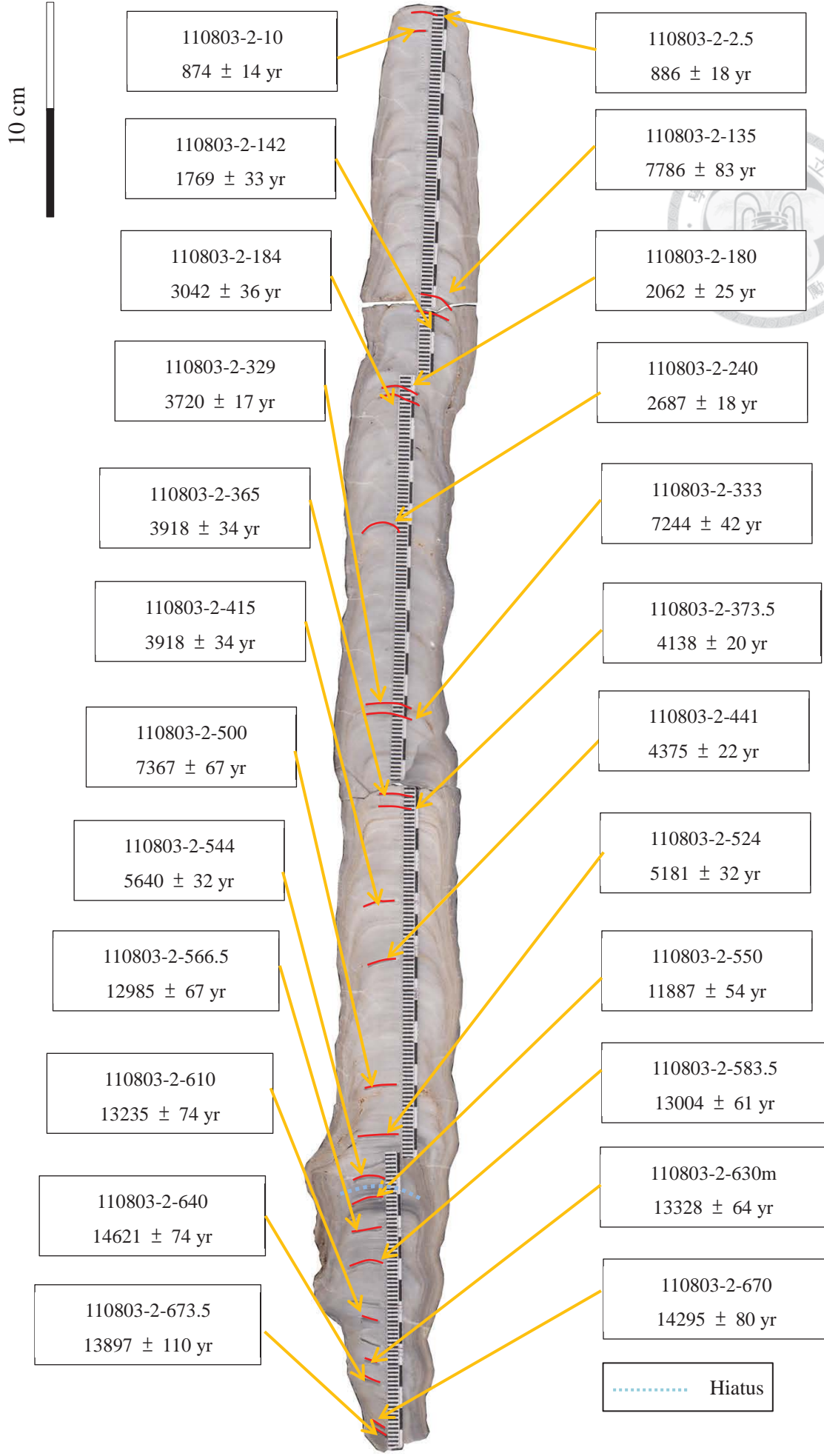


Figure 3-3. Stalagmite MC110803-2



Table 3-3. ^{230}Th age data of stalagmite 090721-2MC.

Sample ID	Depth(mm)	Age (ka)	Error (2σ)
110803-2A-3	3	11.618	0.064
110803-2A-40	40	12.496	0.061
110803-2A-60	60	12.774	0.062
110803-2A-71	71	13.16	0.20

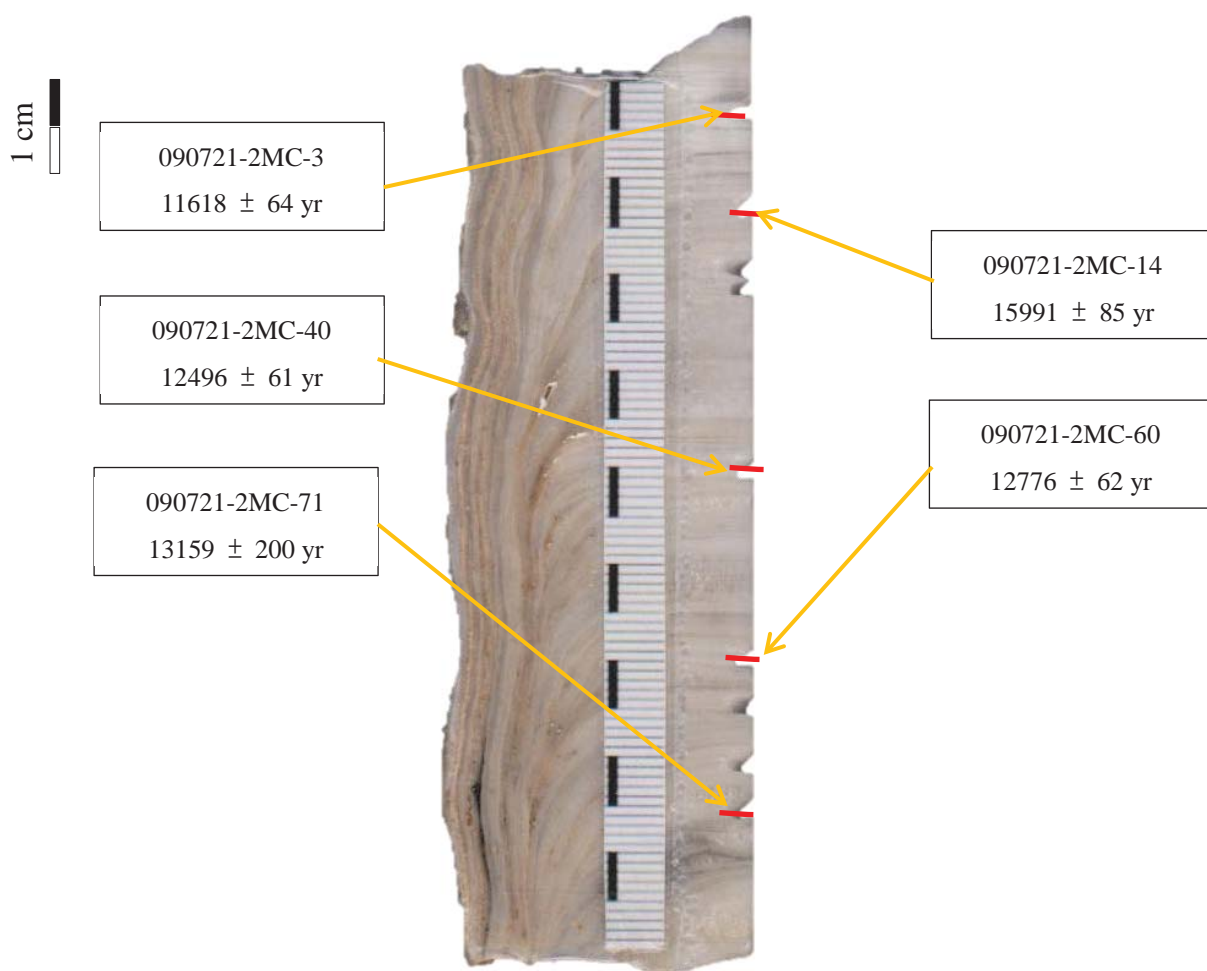


Figure 3-4. Stalagmite 090721-2MC



3.2 Oxygen and carbon stable isotope records

3.2.1 Hendy Test and Replication Test

'Hendy test' (Hendy *et al.*, 1971) was conducted along coeval growth layers, and all layers have less than 0.2‰ of $\delta^{18}\text{O}$ variation (1-sigma) (Fig. 3-5a), showing that stalagmites deposited at an oxygen isotopic equilibrium condition. The R^2 for $\delta^{18}\text{O}$ and $\delta^{13}\text{C}$ value in coeval layers of three selected stalagmites MC110803-1, MC110803-2, and 090721-2MC were depicted respectively by Figs. 3-5b to 3-5d. Several layers $\delta^{18}\text{O}$ and $\delta^{13}\text{C}$ values show high covariance. However, various slopes of **regression lines have little implications of dominant kinetic effect in the Lekiraka cave.** Two contemporaneous $\delta^{18}\text{O}$ records for MC110803-1 and MC110803-2 are well replicated from 0.8 to 5.7ka (Fig. 3-6), combined with robust Hendy Test, this high replication between records suggest that little kinetic fractionation and insignificant influence from water-rock interaction.

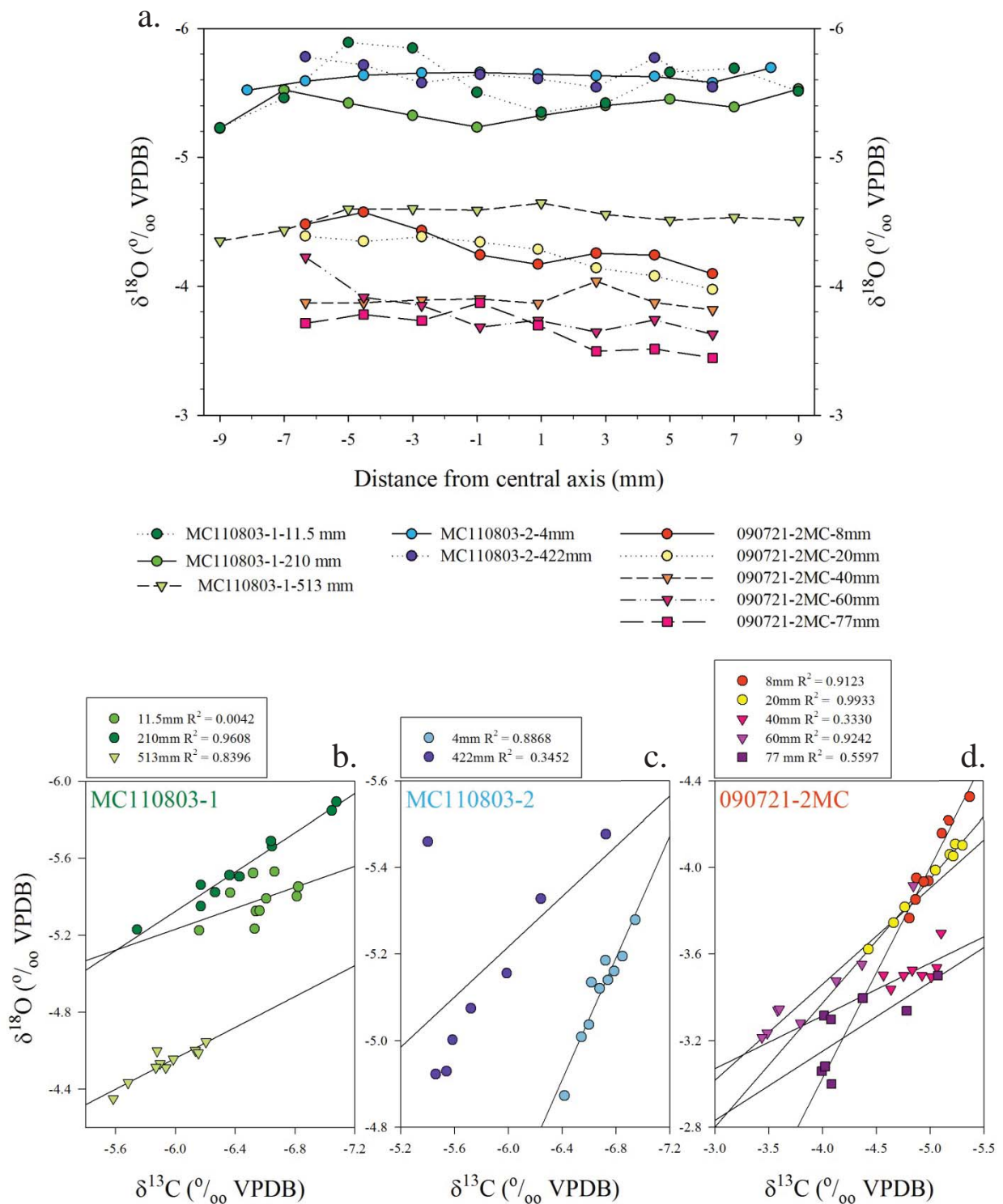


Figure 3-5. Results of ‘Hendy Test’ of Lekiraka stalagmites. (a) Green, blue, and orange symbols denote the results of ‘Hendy Test’ of various stalagmite sections. 1-sigma value of all tested layers are less than 0.2‰, indicate a stable precipitation environment. (b)(c) The linear regressions of subsamples from different stalagmites are subsequently color-coded. Various slopes of regression lines suggest remote possibility of dominant kinetic effect.



3.2.2 Oxygen stable isotope time series

Oxygen stable isotope time series of three selected stalagmites are given in Figure 3-7. $\delta^{18}\text{O}$ values of Lekiraka stalagmite records vary between -4.89‰ and -2.31‰ during 16.5-11.5 ka, -2.94‰ and -6.85‰ during 5.7-3.5 ka. A rapid drop of 1‰ occurred during 5.5 ka – 5.7 ka. This compiled record shows an ^{18}O depletion trend from late Pleistocene to Holocene (Fig 3-7).

Previous studies indicate that deglaciation process would essentially decrease the seawater $\delta^{18}\text{O}$ values for ~1‰ of decreasing (Dykoski *et al.*, 2005; Schrag *et al.*, 1996). We assume that the shift of **sea level** is proportional to $\delta^{18}\text{O}$ change during deglaciation, the reconstructed deglacial sea-level curve (Bard *et al.*, 1996; Fairbanks *et al.*, 1989; Grant *et al.*, 2012; Siddall *et al.*, 2003) can be used to calculate decrease in $\delta^{18}\text{O}$ value of ~0.5‰ during 16 to 11.5 ka, and additional ~0.5‰ decrease during the first half of Holocene (Griffiths *et al.*, 2009). However, the fluctuation of moisture $\delta^{18}\text{O}$ values during transformation of last deglaciation is difficult to be well estimated. The exposure and flooding of Sunda Shelf could bring an unexpected effect on regional atmospheric circulation and alternation of moisture amount and source to our study sites.

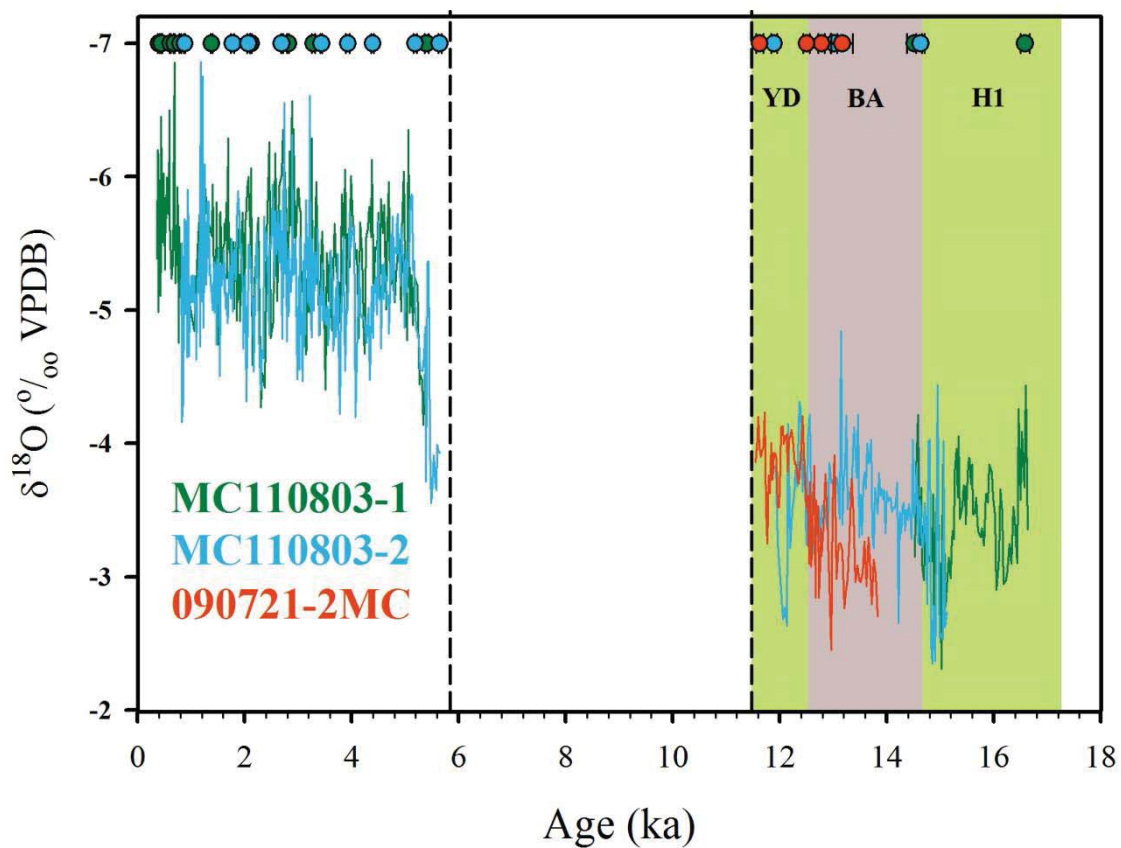


Figure 3-6. $\delta^{18}\text{O}$ records of Lekiraka stalagmites. Green, blue and orange line respectively denote $\delta^{18}\text{O}$ records of stalagmite MC110803-1, MC110803-2, and 090721-2MC. ^{230}Th dates with 2σ error are color-coded with stalagmites. Vertical colorful bars indicate Heinrich event 1 (H1) stadal, Bølling-Allerød (B-A) interstadial, and Younger Dryas (YD) stadal defined in previous studies (Dykoski *et al.*, 2005; Petit *et al.*, 1999; Wang *et al.*, 2001).

Chapter 4 Discussion



4.1 Fluctuation of hydroclimate in Australian-Indonesian monsoon territory since the last 16,500 years

Modern (1952-1974 AD) climate data (Griffiths *et al.*, 2009; National Directorate of Meteorology and Geophysics, Timor-Leste), long-term (1981-2011) regional climatology data (<http://www.esrl.noaa.gov>, Physical Science Division, Earth System Research Laboratory, NOAA), and moisture-source trajectory modeling (Draxler and Rolph, 2013) (Figs. 4-1 to 4-3) show the same hydrological condition in our Lekiraka cave and published Liang Luar cave in Western Flores (Griffiths *et al.*, 2009) (Figs. 4-1 to 4-2). The agreements indicate the rainfall change in Lekiraka and Liang Luar caves is dominantly governed by same climatic condition under the Australian-Indonesian summer monsoon (AISM). The minor offset between Lekiraka and Liang Luar records could be attributed to different travel distance of moisture source and different summer/winter moisture ratios (Figs. 4-3 and 4-4). Therefore, Lekiraka $\delta^{18}\text{O}$ record is highly consistent with that of Liang Luar (Griffiths *et al.*, 2009), with similar peak at Younger Dryas (YD) stadial, and relatively low $\delta^{18}\text{O}$ during the Holocene. However, there is a prominent shift of 1‰ of $\delta^{18}\text{O}$ value during 5.5-5.7 ka, which could be attributed to recrystallization process of the stalagmites.

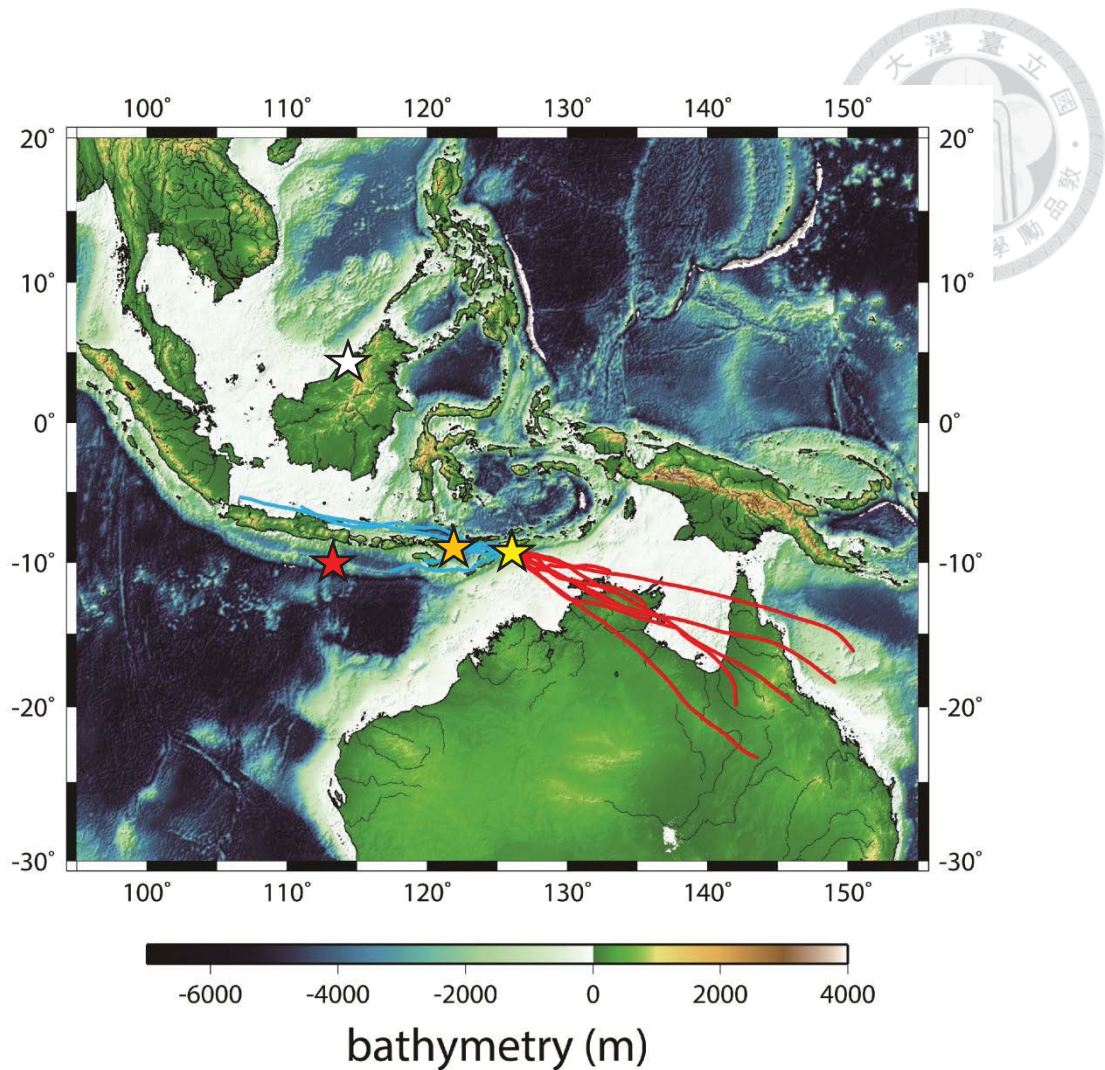


Figure 4-1. Map showing site locations and moisture trajectories. Stars mark the cave locations of Lekiraka cave (yellow, this study), Liang Luar cave in Western Flores (orange) (Griffiths *et al.*, 2009), Bukit Assam and Snail Shell caves in Gunung Buda National Park in Borneo (white) (Partin *et al.*, 2007), and also a marine sediment core GeoB10053-7 in the eastern Indian Ocean (red) (Mohtadi *et al.*, 2011). Solid lines represent five-year average (2007-2011 AD) moisture trajectories of Lekiraka cave that were constructed by the HYSPLIT moisture trajectory model (Draxler and Rolph, 2013). Blue lines represent the moisture trajectories for rainy season (December – March), and red lines represent moisture trajectories for the other months from April to November.

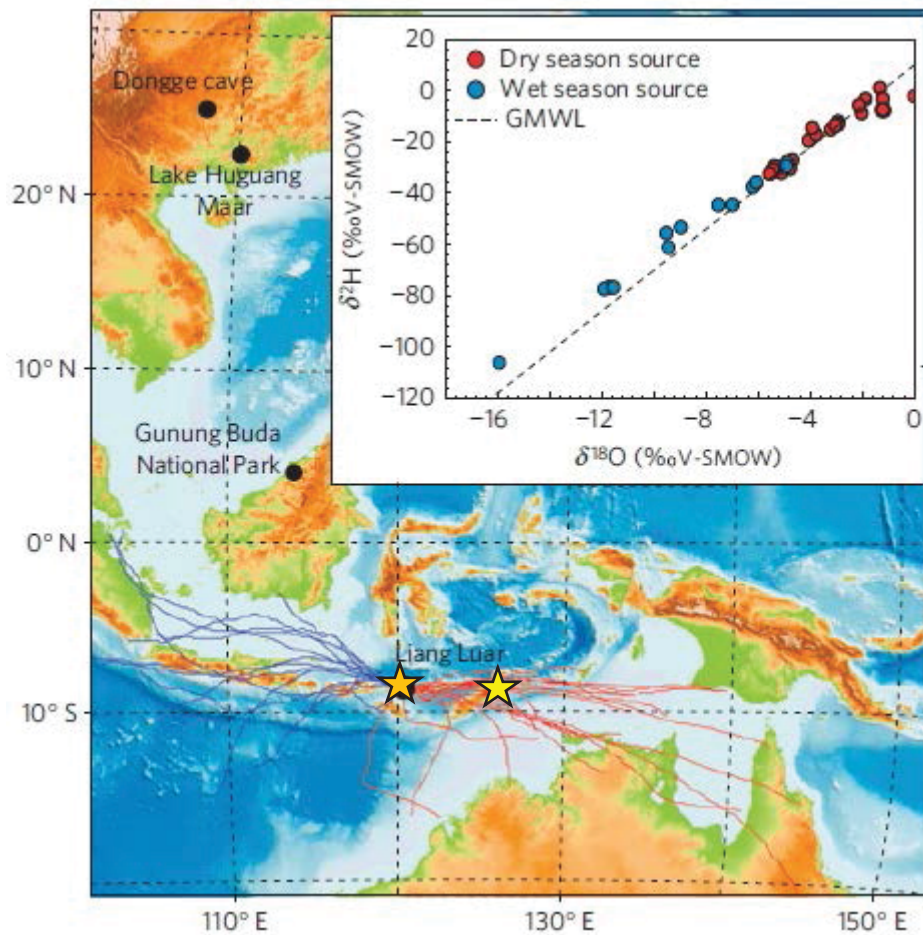


Figure 4-2. Moisture trajectories for Laing Luar cave (orange star, Griffiths *et al.*, 2009). Stars mark the cave locations of Lekiraka cave (yellow, this study), Liang Luar cave in Western Flores (orange) (Griffiths *et al.*, 2009). Solid lines represent moisture trajectories (September 2006 – April 2007) of Liang Luar cave that were constructed by the HYSPLIT moisture trajectory model (Draxler and Rolph, 2013). Blue lines represent the moisture trajectories for rainy season (December - March), and red lines represent moisture trajectories for dry season (June - August) (Modified from Griffiths *et al.*, 2009).

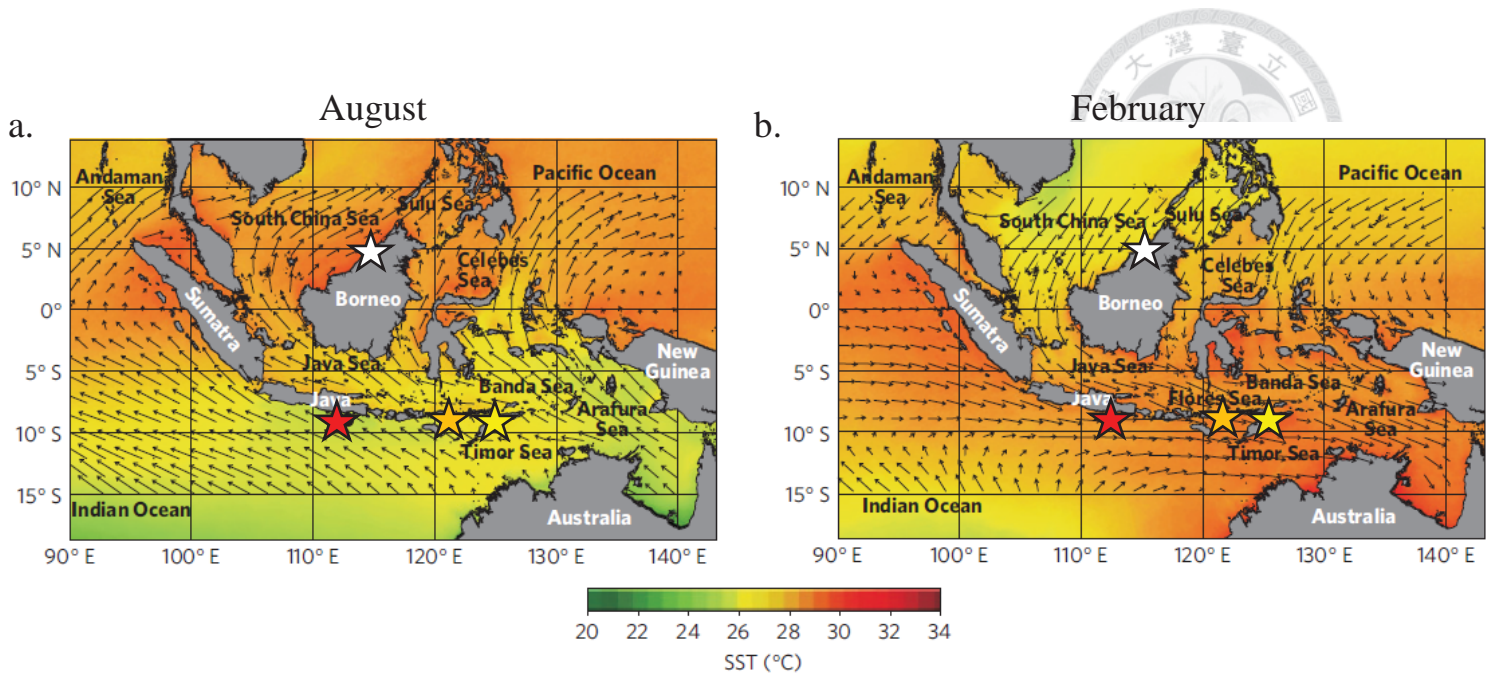


Figure 4-3. Map showing site locations and seasonal climate information. Remote-sensing SST data are averaged from January 2002 to February 2008 (Aqua MODIS, <http://oceancolor.gsfc.nasa.gov>). Stars mark the cave locations of Lekiraka cave (yellow, this study), Liang Luar cave in Western Flores (orange) (Griffiths *et al.*, 2009), Bukit Assam and Snail Shell caves in Gunung Buda National Park in Borneo (white) (Partin *et al.*, 2007), and also a marine sediment core GeoB10053-7 in the eastern Indian Ocean (red) (Mohtadi *et al.*, 2011). Superimposed black arrows indicate the intensity and direction of scatterometer wind in (a) August and (b) February (Modified from Mohtadi *et al.*, 2011).

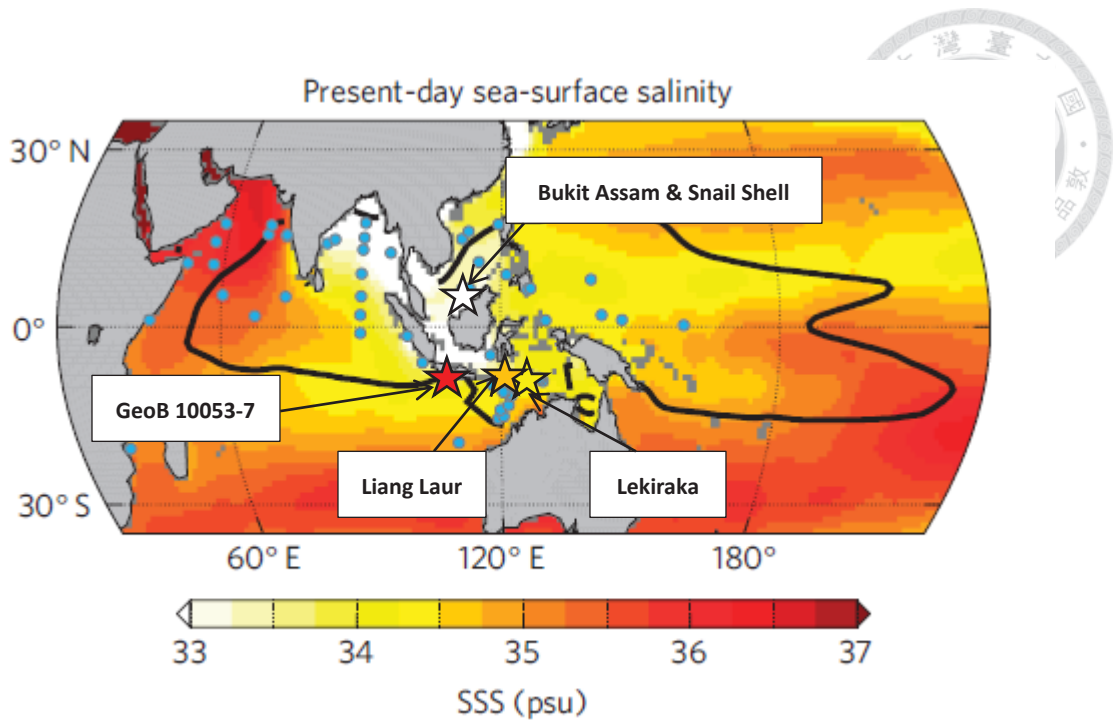
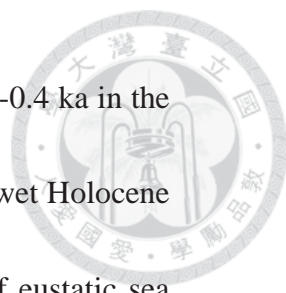


Figure 4-4. Present-day IPWP hydroclimate. Observed mean annual sea surface salinity (SSS) (Antonov *et al.*, 2009). Solid black contour indicates the IPWP boundaries as defined by the annual mean sea surface temperature $> 28^{\circ}\text{C}$ (Reynolds, 2002). Dots denote the locations of marine proxy records used in DiNezio *et al.* (2013).



A prominent $\delta^{18}\text{O}$ shift of 1.8‰ between 16.5-11.5 ka and 5.7-0.4 ka in the spliced Lekiraka record indicates a relatively dry glacial period and wet Holocene in East Timor. This results generally correspond to the up-rising of eustatic sea level since the last glacial maximum (Grant *et al.*, 2012; Hanebuth, Stattegger and Grootes 2000; Hanebuth *et al.*, 2011; Sathiamurthy, 2006; Sidall *et al.*, 2003). However, in sediment records from core GeoB10053-7 (Mohtadi *et al.*, 2011) (Fig. 4-5), millennial-scale events left relatively clear signatures in its AISM records, and the AISM strengthen rapidly in late Holocene. Lekiraka and Liang Luar records have a constant of about 1‰ offset, which could be attributed to different ratios of moisture (Fig. 4-1 to Fig. 4-4). The inconsistency between ocean sediment records and stalagmite records could be attributed to complex rainfall mechanism in this area (DiNezio *et al.*, 2013; Griffiths *et al.*, 2010; Mohtadi *et al.*, 2011). Compare Lekiraka and Liang Luar records to planktonic foraminiferal $\Delta^{18}\text{O}$ -inferred Australian-Indonesian winter monsoon (AIWM) records of GeoB10053-7, highly consistent pattern could be observed (Fig. 4-5). The anti-phasing relationship between GeoB10053-7 AIWM records and Liang Luar / Lekiraka $\delta^{18}\text{O}$ records could be attributed to the “pull-push” mechanism between the AIM and the EAM (An *et al.*, 2000; Rohling *et al.*, 2009).

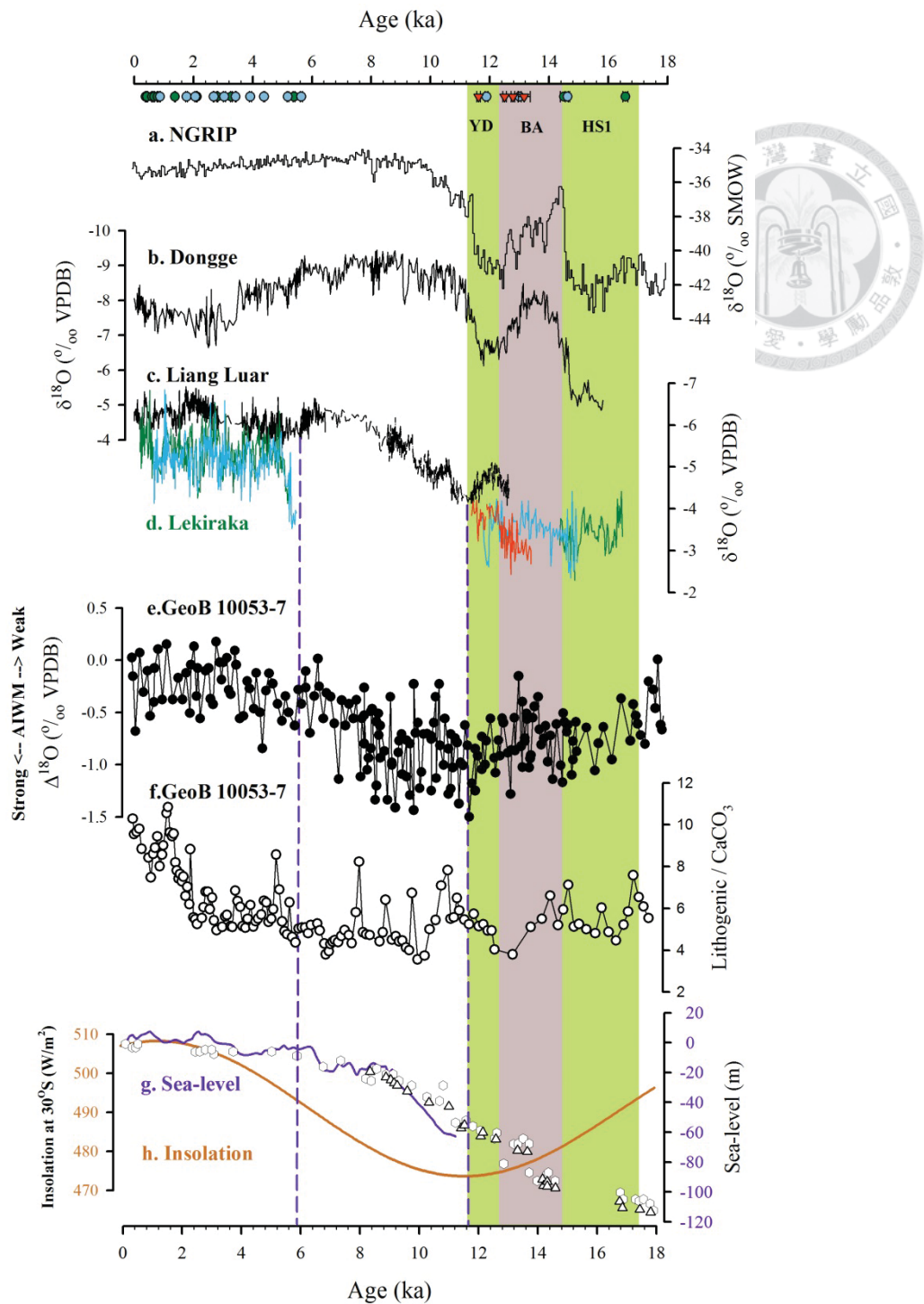


Figure 4-5. Paleoclimate proxy records over the past 18,000 years. (a) $\delta^{18}\text{O}$ record of NGRIP ice core, Greenland (North Greenland Ice Core Project members, 2004). (b) $\delta^{18}\text{O}$ record of Dongge cave, China (Dykoski *et al.*, 2005). (c) $\delta^{18}\text{O}$ record of Liang Luar cave, Flores, Indonesia (Griffiths *et al.*, 2009). (d) $\delta^{18}\text{O}$ record of Lekiraka cave, East Timor (colored line). (e) (f) $\Delta^{18}\text{O}$ and Lithogenic/ CaCO_3 record of sediment core GeoB 10053-7, offshore Java (Mohtadi *et al.*, 2011). (g) Sea-level reconstruction (Sidall *et al.*, 2003). (h) Insolation intensity of 30°S (January).



4.2 Comparison with global and regional paleoclimate proxy records

4.2.1 Late Pleistocene --- From H1 to YD

A dry/cold YD condition shown by significant increase of $\delta^{18}\text{O}$ value in the Asian monsoon (AM) territory stalagmite records (Dykoski *et al.*, 2005; Hu *et al.*, 2008; Jiang *et al.*, 2012; Wang *et al.*, 2001) is absent in Lekiraka and Laing Luar records. Instead, a slightly wet/warm YD condition could be observed in Lekiraka and Laing Luar records (Griffiths *et al.*, 2009), corresponded to intensification of the East Asian Winter monsoon (EAWM) (Yancheva *et al.*, 2007). Assuming monsoon moisture trajectories were broadly similar to present time, a large proportion of summer monsoon trajectory would have been occupied by land during late Pleistocene (Grant *et al.*, 2012; Hanebuth *et al.*, 2011; Sathiamurthy, 2006; Sidall *et al.*, 2003) in Maritime Continent region. Limited moisture availability of source moisture greatly confined the development of AISM, which suggests that southern displacement of the mean ITCZ position should be responsible for increasing rainfall over research sites during YD, agreed with modeling results (Dykoski *et al.*, 2005; Griffiths *et al.*, 2009; Yancheva *et al.*, 2007; Zhang and Delworth, 2005).

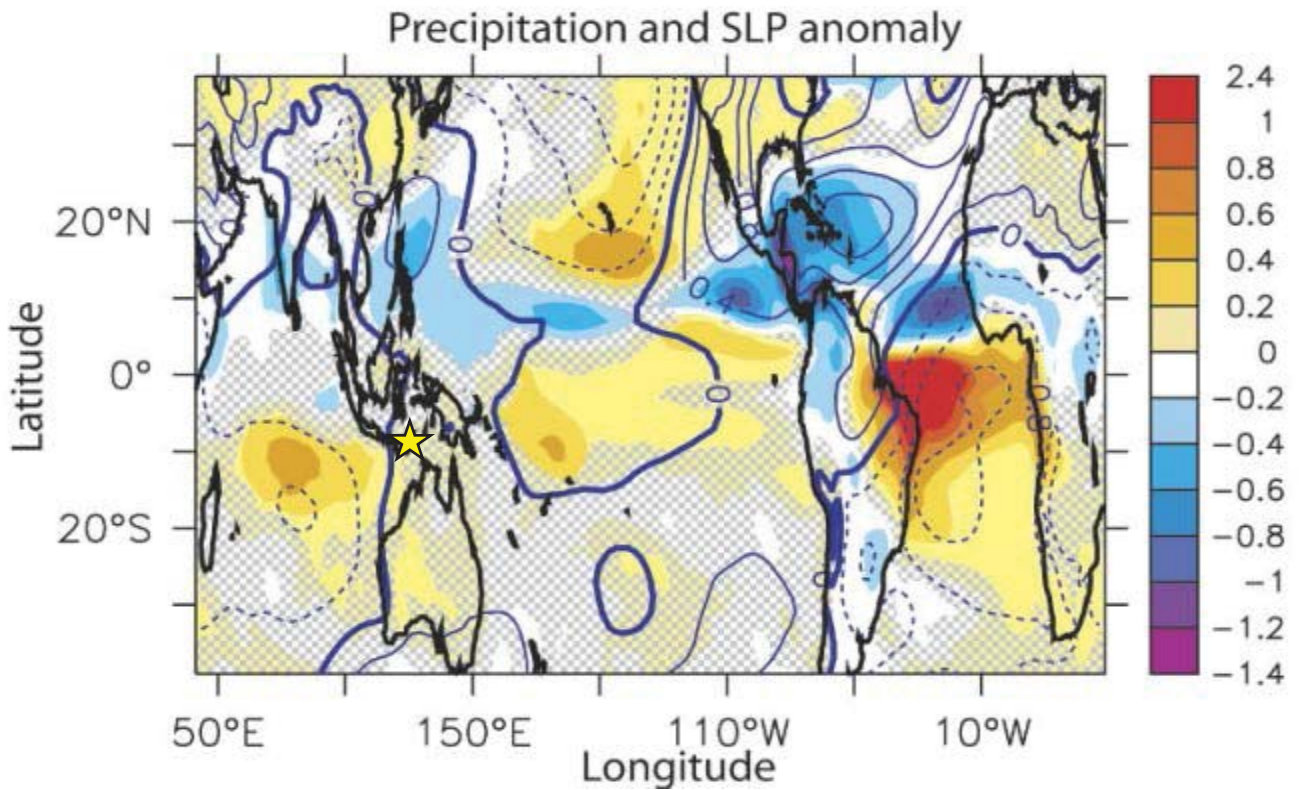
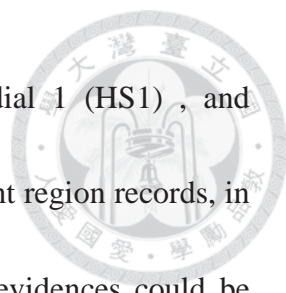


Figure 4-6. Simulation result of the fully coupled ocean-atmosphere global general circulation model (CM2.0) with the slab ocean model. Simulated annual mean precipitation anomaly (m/yr) base on thermohaline reduction scenario, a slightly positive precipitation anomaly can be observed over the Southern Indian Ocean and the Southern Pacific. Yellow star denote the location of Lekiraka cave (this study). The blue contour is the annual mean sea level pressure (SLP) anomaly with an interval of 0.4 hPa (Modified from Zhang and Delworth, 2005).



Millennium scale climate events such as YD, Heinrich stadial 1 (HS1), and Bølling-Allerød (B-A) interstadial, are ‘muted’ in Maritime Continent region records, in contrast to NH low latitude paleoclimate records (Fig 4-5). Few evidences could be found that the insolation intensity and sea-level change during H1 to B-A were responsible for this phenomenon. Sea surface temperature (SST), a complementary factor, should be involved. According to modeling results, reduced zonal tropical Indo-Pacific Ocean SST gradient and/or Sunda Shelf exposure could induce slowdown and/or displacement in the Walker circulation (Fig. 4-6 to Fig. 4-9) (DiNezio *et al.*, 2013; Sathiamurthy, 2006; Tokinaga *et al.*, 2012; Zhang and Delworth, 2005). SST records over the IPWP since the last glacial maximum (LGM) were reconstructed by multiple ocean sediment cores, and constant warming since the LGM could be observed throughout IPWP region (Kiefer and Kienast, 2005; Rosenthal *et al.*, 2003; Stott *et al.*, 2004; Visser, Thunell and Stott 2003; Xu *et al.*, 2010), suggesting that the SST fluctuation, as well as eustatic sea-level change, could be critical to the past precipitation history for Maritime Continent region.

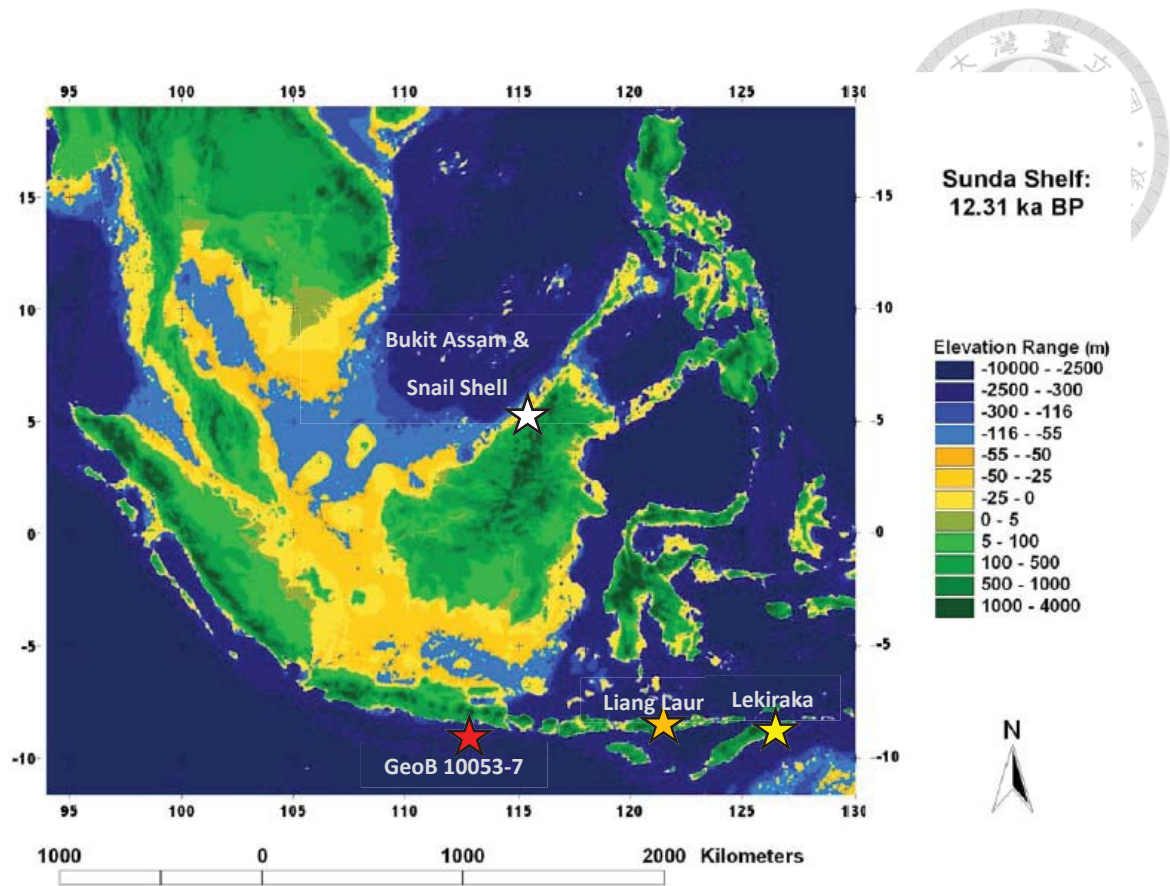


Figure 4-7. Reconstruction of Sunda shelf eustatic sea-level during at 12.31 ka BP (Sathiamurthy, 2006). At 12.31 ka BP, Sunda Shelf was about 50m - 55m below present day sea-level (Modified from Sathiamurthy, 2006). Yellow, orange, white, and red stars respectively denote the locations of Lekiraka cave (this study), Laing Luar cave (Griffiths *et al.*, 2009), Bukit Assam and Snail Shell cave (Partin *et al.*, 2007), and sediment core GeoB 10053-7 (Mohtadi *et al.*, 2011).

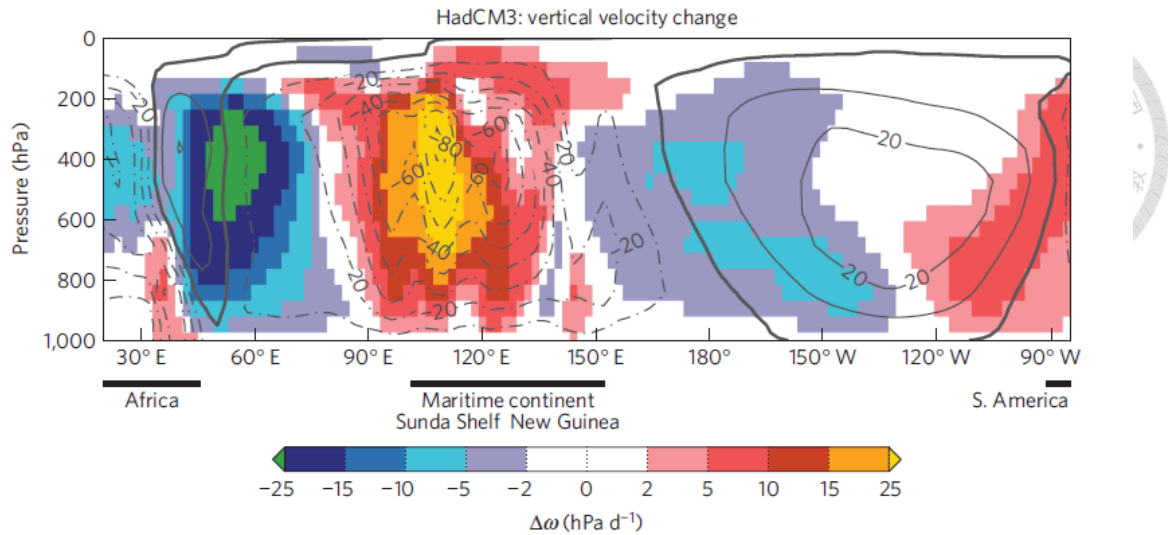


Figure 4-8. Simulated Indo-Pacific Walker circulation change in the LGM. Changes in vertical velocity (ω) over the equatorial Indo-Pacific simulated by HadCM3 in response to the LGM forcing (colors). Contours are annual-mean ω simulated in the pre-industrial control experiment (DiNezio *et al.*, 2013).

HadCM3 simulated rainfall and salinity change DJF and JJA

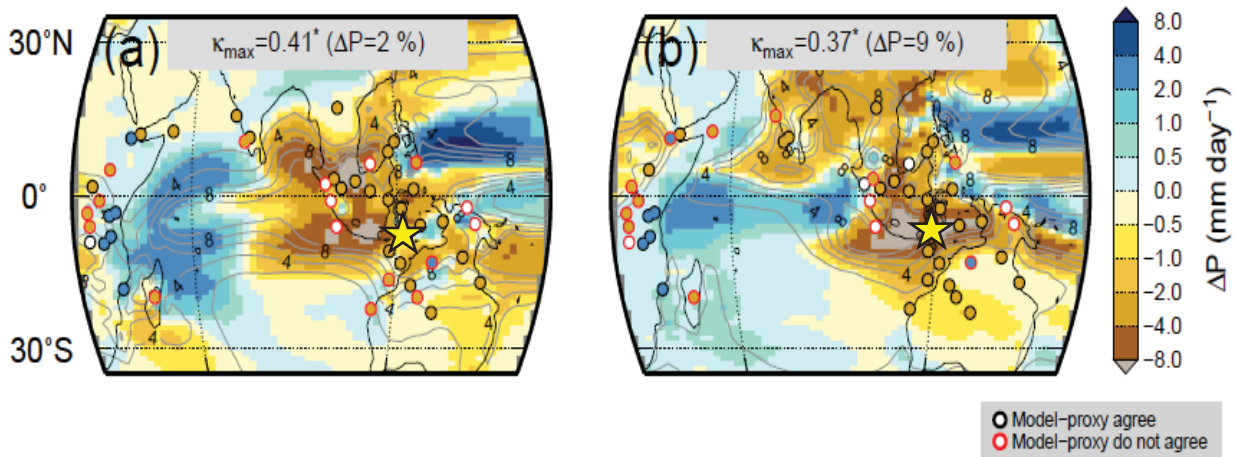


Figure 4-9. Simulated LGM changes in the Indo-Pacific. Change in precipitation during (a) austral summer (DJF) and (b) austral winter (JJA) simulated by HadCM3 in response to the LGM forcing. Yellow stars denote the location of Lekiraka cave (this study). The coastlines correspond to the 120 m isobaths of the present day ocean bathymetry (modified from DiNezio *et al.*, 2013).

4.2.2 Middle to Late Holocene

The Sunda Shelf has been fully flooded since the early Holocene (Hanebuth, Statterger and Grootes 2000; Hanebuth *et al.*, 2011; Sathiamurthy, 2006); thus, minor eustatic sea-level fluctuation no longer dominated the regional hydroclimate. Little evidence indicates that the ITCZ mean position or other cross equatorial climate forcing was responsible for centennial to decadal perturbation in low-latitude paleoclimate records (Fig 4-10). Stable regional IPWP SST during the Holocene (Visser, Thunell and Stott 2003; Stott *et al.*, 2004) implies that there could be an insignificant variation in the adjacent terrestrial records. Two speculations attribute to the regional inconsistent short-term perturbation: First, the AIM system has a complex and nonlinear respond to regional climate forcing (Mohtadi *et al.*, 2011; DiNezio *et al.*, 2013); second, local components such as environment or geographical characteristic of cave sites are rather notable for paleoclimate proxy records in a relative short time perspective (Fairchild *et al.*, 2006; Lachiniet *et al.*, 2009).



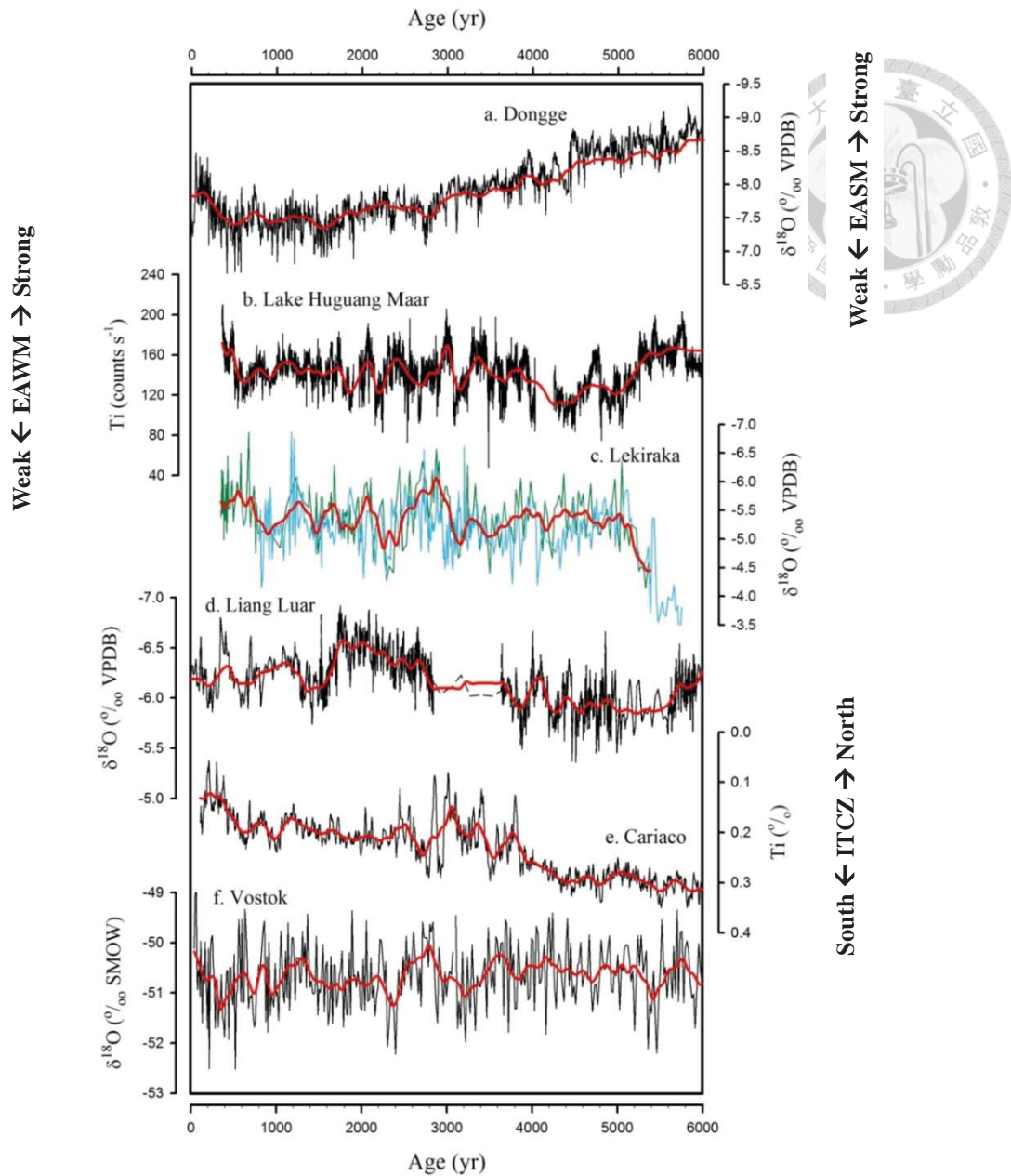


Figure 4-10. Paleoclimate proxy records over the past 6,000 years. (a) $\delta^{18}\text{O}$ record of Dongge cave, China (Dykoski *et al.*, 2005). (b) Ti concentration record of Lake Huguang Maar, China (Yancheva *et al.*, 2007). (c) $\delta^{18}\text{O}$ record of Lekiraka cave, East Timor (colored line). (d) $\delta^{18}\text{O}$ record of Liang Luar cave, Flores, Indonesia (Griffiths *et al.*, 2009). (e) Ti concentration record of Cariaco Basin (Haug *et al.*, 2001). (f) $\delta^{18}\text{O}$ record of Vostok ice core (Petit *et al.*, 1999). Red lines denote the 5-point average of each proxy records respectively.

Chapter 5 Conclusions



1. Stalagmite $\delta^{18}\text{O}$ records and modern local hydroclimate condition of the Lekiraka cave are highly consistent with that of the Liang Luar cave (Griffiths *et al.*, 2009). It indicates that East Timor and Flores have experienced the same climate variation in the past. Agreement of stalagmite records between two sites also suggests that the Lekiraka records can be interpreted as a proxy of the AISM over the last glacial-interglacial period.
2. The evolution of Lekiraka $\delta^{18}\text{O}$ records could be attributed to: (1) fluctuation of the AISM activity, (2) migration of the ITCZ, and (3) eustatic sea-level change.
3. The dynamic and inter-connected behavior of the IPWP, the AM and AIM systems since the LGM highlights the fundamental importance of the warm pool region for understanding climate change throughout the tropics.
4. Inconsistency between marine and terrestrial paleoclimate records in AIM territory is likely contributed to complex regional rainfall mechanism.
5. Detailed mechanism of how the Sunda Shelf exposure would affect the regional atmospheric circulation is still unclear. More high-resolution terrestrial, marine proxy records and model simulations are required.

Reference



Antonov, J. I. (2009) *World Ocean Atlas, Salinity*, 2, 184.

Abram, N. J., M. K. Gagan, Z. Liu, W. S. Hantoro, M. T. McCulloch & B. W.

Suwargadi (2007) Seasonal characteristics of the Indian Ocean Dipole during the Holocene epoch. *Nature*, 445, 299-302.

Abram, N. J., H. V. McGregor, M. K. Gagan, W. S. Hantoro & B. W. Suwargadi (2009)

Oscillations in the southern extent of the Indo-Pacific warm pool during the mid-Holocene. *Quaternary Science Reviews*, 28, 2794-2803.

An, Z. S. (2000) The history and variability of the East Asian paleomonsoon climate.

Quaternary Science Reviews, 19, 171-187.

Bard, E., B. Hamelin, M. Arnold, L. Montaggioni, G. Cabioch, G. Faure & F. Rougerie

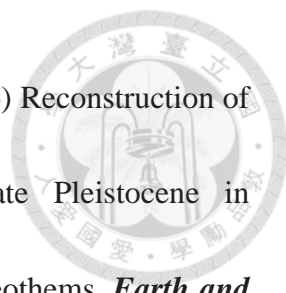
(1996) Deglacial sea-level record from Tahiti corals and the timing of global meltwater discharge. *Nature*, 382, 241-244.

Barker, S., P. Diz, M. J. Vautravers, J. Pike, G. Knorr, I. R. Hall & W. S. Broecker (2009)

Interhemispheric Atlantic seesaw response during the last deglaciation. *Nature*, 457, 1097-U50.

Blunier, T. & E. J. Brook (2001) Timing of millennial-scale climate change in

Antarctica and Greenland during the Last Glacial Period. *Science*, 291, 109-112.



Cruz, F. W., S. J. Burns, I. Karmann, W. D. Sharp & M. Vuille (2006) Reconstruction of regional atmospheric circulation features during the late Pleistocene in subtropical Brazil from oxygen isotope composition of speleothems. *Earth and Planetary Science Letters*, 248, 495-507.

Cruz, F. W., M. Vuille, S. J. Burns, X. F. Wang, H. Cheng, M. Werner, R. L. Edwards, I. Karmann, A. S. Auler & H. Nguyen (2009) Orbitally driven east-west antiphasing of South American precipitation. *Nature Geoscience*, 2, 210-214.

Denton, G. H., R. F. Anderson, J. R. Toggweiler, R. L. Edwards, J. M. Schaefer & A. E. Putnam (2010) The Last Glacial Termination. *Science*, 328, 1652-1656.

DiNezio, P. N. & J. E. Tierney (2013) The effect of sea level on glacial Indo-Pacific climate. *Nature Geoscience*, 6, 485-491.

Dorale, J. A. & Z. H. Liu (2009) Limitations of Hendy Test criteria in judging the paleoclimatic suitability of speleothems and the need for replication. *Journal of Cave and Karst Studies*, 71, 73-80.

Draxler, R. R. & Rolph (2013), G. D. HYSPLIT4 Hybrid Single-Particle Lagrangian Integrated Trajectory Model <<http://www.arl.noaa.gov/ready/hysplit4.html>>.

Dykoski, C. A., R. L. Edwards, H. Cheng, D. X. Yuan, Y. J. Cai, M. L. Zhang, Y. S. Lin, J. M. Qing, Z. S. An & J. Revenaugh (2005) A high-resolution, absolute-dated Holocene and deglacial Asian monsoon record from Dongge Cave, China. *Earth*



and Planetary Science Letters, 233, 71-86.

Fairbanks, R. G. (1989) A 17,000-year glacio-eustatic sea-level record - influence of glacial melting rates on the Younger Dryas event and deep-ocean circulation.

Nature, 342, 637-642.

Fairchild, I. J., C. L. Smith, A. Baker, L. Fuller, C. Spotl, D. Matthey, F. McDermott & Eimp (2006) Modification and preservation of environmental signals in speleothems. *Earth-Science Reviews*, 75, 105-153.

Fleitmann, D., S. J. Burns, U. Neff, M. Mudelsee, A. Mangini & A. Matter (2004) Palaeoclimatic interpretation of high-resolution oxygen isotope profiles derived from annually laminated speleothems from Southern Oman. *Quaternary Science Reviews*, 23, 935-945.

Grant, K. M., E. J. Rohling, M. Bar-Matthews, A. Ayalon, M. Medina-Elizalde, C. B. Ramsey, C. Satow & A. P. Roberts (2012) Rapid coupling between ice volume and polar temperature over the past 150,000 years. *Nature*, 491, 744-747.

Griffiths, M. L., R. N. Drysdale, M. K. Gagan, J. X. Zhao, L. K. Ayliffe, J. C. Hellstrom, W. S. Hantoro, S. Frisia, Y. X. Feng, I. Cartwright, E. S. Pierre, M. J. Fischer & B. W. Suwargadi (2009) Increasing Australian-Indonesian monsoon rainfall linked to early Holocene sea-level rise. *Nature Geoscience*, 2, 636-639.

Hanebuth, T., K. Statterger & P. M. Grootes (2000) Rapid flooding of the Sunda Shelf:



a late-glacial sea-level record. *Science*, 288, 1033-1035.

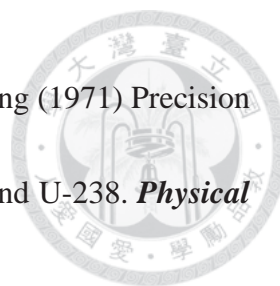
Hanebuth, T. J. J., H. K. Voris, Y. Yokoyama, Y. Saito & J. Okuno (2011) Formation and fate of sedimentary depocentres on Southeast Asia's Sunda Shelf over the past sea-level cycle and biogeographic implications. *Earth-Science Reviews*, 104, 92-110.

Haug, G. H., K. A. Hughen, D. M. Sigman, L. C. Peterson & U. Rohl (2001) Southward migration of the intertropical convergence zone through the Holocene. *Science*, 293, 1304-1308.

Hendy, C. H. (1971) The isotopic geochemistry of speleothems—I. The calculation of the effects of different modes of formation on the isotopic composition of speleothems and their applicability as palaeoclimatic indicators. *Geochimica et Cosmochimica Acta*, 35, 801-824.

Holbourn, A., W. Kuhnt, H. Kawamura, Z. M. Jian, P. Grootes, H. Erlenkeuser & J. Xu (2005) Orbitally paced paleoproductivity variations in the Timor Sea and Indonesian Throughflow variability during the last 460 kyr. *Paleoceanography*, 20.

Hu, C. Y., G. M. Henderson, J. H. Huang, S. Xie, Y. Sun & K. R. Johnson (2008) Quantification of Holocene Asian monsoon rainfall from spatially separated cave records. *Earth and Planetary Science Letters*, 266, 221-232.



Jaffey, A. H., K. F. Flynn, Glendeni.Le, W. C. Bentley & A. M. Essling (1971) Precision measurement of half-Lives and specific activities of U-235 and U-238. *Physical Review C*, 4, 1889-&.

Jiang, X. Y., Y. Q. He, C. C. Shen, X. G. Kong, Z. Z. Li & Y. W. Chang (2012) Stalagmite-inferred Holocene precipitation in northern Guizhou Province, China, and asynchronous termination of the Climatic Optimum in the Asian monsoon territory. *Chinese Science Bulletin*, 57, 795-801.

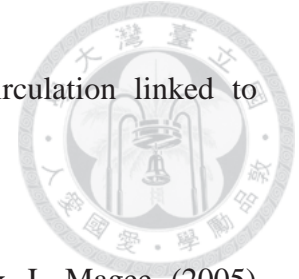
Kershaw, A. P., S. van der Kaars & P. T. Moss (2003) Late Quaternary Milankovitch-scale climatic change and variability and its impact on monsoonal Australasia. *Marine Geology*, 201, 81-95.

Kiefer, T. & M. Kienast (2005) Patterns of deglacial warming in the Pacific Ocean: a review with emphasis on the time interval of Heinrich event 1. *Quaternary Science Reviews*, 24, 1063-1081.

Lachniet, M. S. (2009) Climatic and environmental controls on speleothem oxygen-isotope values. *Quaternary Science Reviews*, 28, 412-432.

Linsley, B. K., Y. Rosenthal & D. W. Oppo (2010) Holocene evolution of the Indonesian throughflow and the western Pacific warm pool. *Nature Geoscience*, 3, 578-583.

McManus, J. F., R. Francois, J. M. Gherardi, L. D. Keigwin & S. Brown-Leger (2004)



Collapse and rapid resumption of Atlantic meridional circulation linked to deglacial climate changes. *Nature*, 428, 834-837.

Miller, G., J. Mangan, D. Pollard, S. Thompson, B. Felzer & J. Magee (2005)

Sensitivity of the Australian Monsoon to insolation and vegetation: Implications for human impact on continental moisture balance. *Geology*, 33, 65-68.

Mohtadi, M., D. W. Oppo, S. Steinke, J. B. W. Stuut, R. De Pol-Holz, D. Hebbeln & A.

Luckge (2011) Glacial to Holocene swings of the Australian-Indonesian monsoon. *Nature Geoscience*, 4, 540-544.

North Greenland Ice Core Project members. (2004) High-resolution record of Northern

Hemisphere climate extending into the last interglacial period. *Nature*, 431, 7005, 147-151.

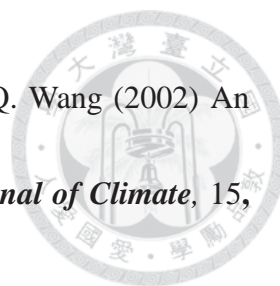
Partin, J. W., K. M. Cobb, J. F. Adkins, B. Clark & D. P. Fernandez (2007) Stalagmite

records of tropical pacific climate since the last glacial maximum. *Geochimica Et Cosmochimica Acta*, 71, A760-A760.

Petit, J. R., J. Jouzel, D. Raynaud, N. I. Barkov, J. M. Barnola, I. Basile, M. Bender, J.

Chappellaz, M. Davis, G. Delaygue, M. Delmotte, V. M. Kotlyakov, M. Legrand, V. Y. Lipenkov, C. Lorius, L. Pepin, C. Ritz, E. Saltzman & M. Stievenard (1999)

Climate and atmospheric history of the past 420,000 years from the Vostok ice core, Antarctica. *Nature*, 399, 429-436.



Reynolds, R. W., N. A. Rayner, T. M. Smith, D. C. Stokes & W. Q. Wang (2002) An improved in situ and satellite SST analysis for climate. *Journal of Climate*, 15, 1609-1625.

Rohling, E. J., Q. S. Liu, A. P. Roberts, J. D. Stanford, S. O. Rasmussen, P. L. Langen & M. Siddall (2009) Controls on the East Asian monsoon during the last glacial cycle, based on comparison between Hulu Cave and polar ice-core records. *Quaternary Science Reviews*, 28, 3291-3302.

Rosenthal, Y., D. W. Oppo & B. K. Linsley (2003) The amplitude and phasing of climate change during the last deglaciation in the Sulu Sea, western equatorial Pacific. *Geophysical Research Letters*, 30.

Sathiamurthy, E., H. K. Voris (2006) Maps of Holocene Sea Level Transgression and Submerged Lakes on the Sunda Shelf. *The Natural History Journal of Chulalongkorn University*, Supplement 2: 1-43

Schrag, D. P., G. Hampt & D. W. Murray (1996) Pore fluid constraints on the temperature and oxygen isotopic composition of the glacial ocean. *Science*, 272, 1930-1932.

Shen, C.C., C.C. Wu, H. Cheng, R. Lawrence Edwards, Y.-T. Hsieh, S. Gallet, C.-C.

Chang, T.-Y. Li, D. D. Lam, A. Kano, M. Hori & C. Spötl (2012) High-precision and high-resolution carbonate ^{230}Th dating by MC-ICP-MS with SEM

protocols. *Geochimica et Cosmochimica Acta*, 99, 71-86.

Shen, C. C., H. Cheng, R. L. Edwards, S. B. Moran, H. N. Edmonds, J. A. Hoff & R. B.

Thomas (2003) Measurement of attogram quantities of Pa-231 in dissolved and particulate fractions of seawater by isotope dilution thermal ionization mass spectroscopy. *Analytical Chemistry*, 75, 1075-1079.

Siddall, M., E. J. Rohling, A. Almogi-Labin, C. Hemleben, D. Meischner, I. Schmelzer

& D. A. Smeed (2003) Sea-level fluctuations during the last glacial cycle. *Nature*, 423, 853-858.

Stenni, B., D. Buiron, M. Frezzotti, S. Albani, C. Barbante, E. Bard, J. M. Barnola, M.

Baroni, M. Baumgartner, M. Bonazza, E. Capron, E. Castellano, J. Chappellaz,

B. Delmonte, S. Falourd, L. Genoni, P. Iacumin, J. Jouzel, S. Kipfstuhl, A.

Landais, B. Lemieux-Dudon, V. Maggi, V. Masson-Delmotte, C. Mazzola, B.

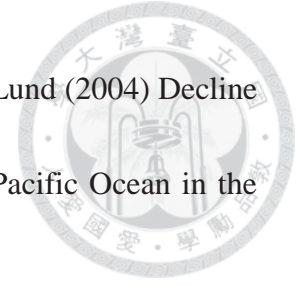
Minster, M. Montagnat, R. Mulvaney, B. Narcisi, H. Oerter, F. Parrenin, J. R.

Petit, C. Ritz, C. Scarchilli, A. Schilt, S. Schupbach, J. Schwander, E. Selmo, M.

Severi, T. F. Stocker & R. Udisti (2011) Expression of the bipolar see-saw in Antarctic climate records during the last deglaciation. *Nature Geoscience*, 4, 46-49.

Stott, L. (2002) Super ENSO and global climate oscillations at millennial time scales

(vol 297, pg 222, 2002). *Science*, 298, 751-751.



Stott, L., K. Cannariato, R. Thunell, G. H. Haug, A. Koutavas & S. Lund (2004) Decline of surface temperature and salinity in the western tropical Pacific Ocean in the Holocene epoch. *Nature*, 431, 56-59.

Tokinaga, H., S. P. Xie, C. Deser, Y. Kosaka & Y. M. Okumura (2012) Slowdown of the Walker circulation driven by tropical Indo-Pacific warming. *Nature*, 491, 439-+.

Tudhope, A. W., C. P. Chilcott, M. T. McCulloch, E. R. Cook, J. Chappell, R. M. Ellam, D. W. Lea, J. M. Lough & G. B. Shimmield (2001) Variability in the El Nino - southern oscillation through a glacial-interglacial cycle. *Science*, 291, 1511-1517.

Visser, K., R. Thunell & L. Stott (2003) Magnitude and timing of temperature change in the Indo-Pacific warm pool during deglaciation. *Nature*, 421, 152-155.

Wang, S. Y. & Y. F. Qian (2001) Modeling of the 1998 East Asian summer monsoon by a limited area model with P-sigma incorporated coordinate. *Advances in Atmospheric Sciences*, 18, 209-224.

Wang, X. F., A. S. Auler, R. L. Edwards, H. Cheng, E. Ito & M. Solheid (2006) Interhemispheric anti-phasing of rainfall during the last glacial period. *Quaternary Science Reviews*, 25, 3391-3403.

Wang, Y. J., H. Cheng, R. L. Edwards, Z. S. An, J. Y. Wu, C. C. Shen & J. A. Dorale (2001) A high-resolution absolute-dated late Pleistocene monsoon record from

Hulu Cave, China. *Science*, 294, 2345-2348.

Wyrwoll, K. H., Z. Y. S. Liu, G. Chen, J. E. Kutzbach & X. D. Liu (2007) Sensitivity of the Australian summer monsoon to tilt and precession forcing. *Quaternary Science Reviews*, 26, 3043-3057.

Xu, J. A., W. Kuhnt, A. Holbourn, M. Regenberg & N. Andersen (2010) Indo-Pacific warm pool variability during the Holocene and Last Glacial Maximum. *Paleoceanography*, 25.

Yancheva, G., N. R. Nowaczyk, J. Mingram, P. Dulski, G. Schettler, J. F. W. Negendank, J. Q. Liu, D. M. Sigman, L. C. Peterson & G. H. Haug (2007) Influence of the intertropical convergence zone on the East Asian monsoon. *Nature*, 445, 74-77.

Zhang, R. & T. L. Delworth (2005) Simulated tropical response to a substantial weakening of the Atlantic thermohaline circulation. *Journal of Climate*, 18, 1853-1860.



Appendix (D) Uranium and Thorium isotopic compositions and ^{230}Th ages for East Timor stalagmite samples by MC-ICPMS, Thermo Electron Neptune, at NTU.

Sample ID	Weight g	^{238}U ppb ^a	^{232}Th ppt	$\delta^{234}\text{U}$ measured ^a	$[\text{}^{230}\text{Th}/\text{}^{238}\text{U}]$ activity ^c	$[\text{}^{230}\text{Th}/\text{}^{232}\text{Th}]$ ppm ^d	Age uncorrected	Age corrected ^{c,e}	$\delta^{234}\text{U}_{\text{initial}}$ corrected ^b
090721-2MC-3	0.0726	665.7 ± 1.3	131.9 ± 9.0	25.9 ± 2.7	0.10363 ± 0.00046	8634 ± 629	11,623 ± 64	11,618 ± 64	26.8 ± 2.8
090721-2MC-14	0.0903	525.4 ± 0.7	750.4 ± 7.9	29.0 ± 1.9	0.14057 ± 0.00057	1625 ± 18	16,028 ± 77	15,991 ± 85	30.4 ± 2.0
090721-2MC-40	0.0882	478.53 ± 0.94	373.7 ± 8.0	29.0 ± 2.9	0.11149 ± 0.00037	2357 ± 51	12,516 ± 57	12,496 ± 61	30.0 ± 3.0
090721-2MC-60	0.0908	550.4 ± 1.1	233.9 ± 7.0	34.5 ± 2.7	0.11438 ± 0.00041	4444 ± 147	12,786 ± 61	12,776 ± 62	35.8 ± 2.8
090721-2MC-81	0.0572	591.8 ± 4.5	151 ± 12	66.3 ± 10	0.1213 ± 0.0013	7858 ± 643	13,166 ± 200	13,159 ± 200	69 ± 11
110803-1A-4	0.0448	271.98 ± 0.90	222 ± 10	78.2 ± 4.6	0.01064 ± 0.00023	216 ± 11	1,083 ± 24	1,063 ± 26	78.4 ± 4.6
110803-1A-29	0.0415	282.87 ± 0.29	23 ± 11	82.1 ± 1.4	0.00384 ± 0.00021	765 ± 367	388 ± 21	386 ± 21	82.2 ± 1.4
110803-1A-80	0.0507	314.79 ± 0.53	18.8 ± 9.2	78.4 ± 2.3	0.00437 ± 0.00011	1208 ± 588	444 ± 12	442 ± 12	78.5 ± 2.3
110803-1A-118	0.0785	287.29 ± 0.37	12.0 ± 5.9	84.1 ± 2.0	0.00600 ± 0.00011	2377 ± 1174	606 ± 11	605 ± 11	84.2 ± 2.0
110803-1A-122	0.0951	262.94 ± 0.30	23.0 ± 4.9	85.2 ± 2.1	0.00673 ± 0.00009	1270 ± 270	679 ± 10	677 ± 10	85.4 ± 2.1
110803-1A-153	0.0601	283.51 ± 0.34	22.9 ± 7.7	91.8 ± 1.9	0.00791 ± 0.00013	1617 ± 546	794 ± 13	792 ± 13	92.0 ± 1.9
110803-1B-167	0.0560	303.39 ± 0.45	73.8 ± 8.3	93.3 ± 2.4	0.01374 ± 0.00017	932 ± 105	1,380 ± 18	1,374 ± 18	93.7 ± 2.4
110803-1B-316.5	0.0871	237.87 ± 0.31	43.3 ± 5.3	102.4 ± 2.4	0.02120 ± 0.00015	1922 ± 237	2,120 ± 16	2,115 ± 16	103.0 ± 2.4

Sample ID	Weight g	^{238}U ppb ^a	^{232}Th ppt	$\delta^{234}\text{U}$ measured ^a	$[\text{}^{230}\text{Th}/\text{}^{238}\text{U}]$ activity ^c	$[\text{}^{230}\text{Th}/\text{}^{232}\text{Th}]$ ppm ^d	Age uncorrected	Age corrected ^{c,e}	$\delta^{234}\text{U}$ initial corrected ^b
110803-1B-167	0.0560	303.39 ± 0.45	73.8 ± 8.3	93.3 ± 2.4	0.01374 ± 0.00017	932 ± 105	1,380 ± 18	1,374 ± 18	93.7 ± 2.4
110803-1B-316.5	0.0871	237.87 ± 0.31	43.3 ± 5.3	102.4 ± 2.4	0.02120 ± 0.00015	1922 ± 237	2,120 ± 16	2,115 ± 16	103.0 ± 2.4
110803-1B-361	0.0794	260.28 ± 0.46	108.8 ± 5.8	96.7 ± 2.6	0.02790 ± 0.00016	1102 ± 60	2,813 ± 18	2,803 ± 19	97.4 ± 2.6
110803-1B-366	0.0871	282.37 ± 0.70	122.2 ± 5.3	98.6 ± 3.2	0.03727 ± 0.00020	1422 ± 62	3,767 ± 24	3,756 ± 24	99.6 ± 3.2
110803-1B-447.5	0.0701	261.3 ± 1.0	16.1 ± 6.6	104.5 ± 4.0	0.03265 ± 0.00025	8728 ± 3581	3,275 ± 29	3,274 ± 29	105.5 ± 4.0
110803-1C-635.5	0.0971	259.71 ± 0.42	121.8 ± 4.8	93.7 ± 2.8	0.05285 ± 0.00028	1860 ± 74	5,405 ± 33	5,394 ± 34	95.2 ± 2.9
110803-1C-637.5	0.0659	217.72 ± 0.42	1339.7 ± 7.6	87.8 ± 2.9	0.13687 ± 0.00090	367.3 ± 3.1	14,658 ± 111	14,509 ± 134	91.5 ± 3.0
110803-1C-660	0.1408	287.94 ± 0.41	1874.2 ± 5.2	87.2 ± 1.8	0.16265 ± 0.00092	412.0 ± 2.5	17,632 ± 113	17,474 ± 138	91.7 ± 1.9
110803-1C-690	0.1477	248.65 ± 0.30	766.1 ± 3.4	83.6 ± 1.6	0.15438 ± 0.00067	826.2 ± 5.0	16,727 ± 83	16,652 ± 91	87.7 ± 1.6
110803-1C-740	0.1184	315.58 ± 0.45	189.3 ± 3.9	84.9 ± 1.9	0.13059 ± 0.00068	3590 ± 77	13,963 ± 82	13,948 ± 83	88.3 ± 2.0
110803-1C-789	0.0620	424.1 ± 1.1	504.2 ± 7.5	89.9 ± 3.2	0.15404 ± 0.00057	2139 ± 33	16,605 ± 85	16,576 ± 87	94.2 ± 3.3
110803-1C-800	0.0479	322.87 ± 0.90	133 ± 10	93.1 ± 4.4	0.1446 ± 0.0011	5813 ± 427	15,463 ± 139	15,453 ± 139	97.3 ± 4.6
110803-2A-2.5	0.0527	265.48 ± 0.70	68.4 ± 8.8	91.3 ± 4.6	0.00889 ± 0.00017	570 ± 74	893 ± 18	886 ± 18	91.5 ± 4.6
110803-2A-10	0.0914	251.50 ± 0.47	9.0 ± 5.1	92.2 ± 2.3	0.00872 ± 0.00014	4019 ± 2267	875 ± 14	874 ± 14	92.4 ± 2.3

Sample ID	Weight g	^{238}U ppb ^d	^{232}Th ppt	$\delta^{234}\text{U}$ measured ^e	$[\text{}^{230}\text{Th}/\text{}^{238}\text{U}]$ activity ^c	$[\text{}^{230}\text{Th}/\text{}^{232}\text{Th}]$ ppm ^d	Age uncorrected	Age corrected ^{c,e}	$\delta^{234}\text{U}_{\text{initial}}$ corrected ^b
110803-2A-135	0.1222	257.97 ± 1.30	469.0 ± 4.2	111.5 ± 6.9	0.07698 ± 0.00060	699.2 ± 7.5	7,829 ± 81	7,786 ± 83	114.0 ± 7.1
110803-2A-142	0.1269	297.11 ± 1.46	19.9 ± 3.7	98.2 ± 5.9	0.01767 ± 0.00031	4359 ± 807	1,770 ± 32	1,769 ± 33	98.7 ± 5.9
110803-2A-180	0.1224	176.75 ± 0.74	31.8 ± 3.8	96.9 ± 5.3	0.02057 ± 0.00022	1888 ± 226	2,067 ± 25	2,062 ± 25	97.4 ± 5.4
110803-2A-184	0.1253	225.41 ± 0.64	96.8 ± 3.7	102.2 ± 3.5	0.03039 ± 0.00033	1168 ± 47	3,052 ± 35	3,042 ± 36	103.1 ± 3.5
110803-2A-240	0.1117	267.11 ± 0.29	57.2 ± 4.2	98.9 ± 1.8	0.02677 ± 0.00017	2063.5 ± 150	2,692 ± 18	2,687 ± 18	99.7 ± 1.8
110803-2A-329	0.1202	283.97 ± 0.21	110.7 ± 3.9	96.0 ± 1.3	0.03682 ± 0.00016	1559 ± 55	3,729 ± 17	3,720 ± 17	97.1 ± 1.3
110803-2A-333	0.1195	285.22 ± 0.21	466.0 ± 3.9	94.6 ± 1.2	0.07069 ± 0.00034	714.3 ± 6.9	7,284 ± 37	7,244 ± 42	96.6 ± 1.2
110803-2A-365	0.0946	306.83 ± 0.25	22.8 ± 4.9	100.5 ± 1.5	0.03401 ± 0.00022	7546 ± 1622	3,427 ± 23	3,425 ± 23	101.4 ± 1.5
110803-2B-373.5	0.1303	279.23 ± 0.23	84.5 ± 3.6	100.8 ± 1.3	0.04102 ± 0.00018	2238 ± 95	4,145 ± 19	4,138 ± 20	102.0 ± 1.3
110803-2B-415	0.1250	263.39 ± 0.30	18.8 ± 3.7	96.9 ± 1.3	0.03874 ± 0.00033	8958 ± 1773	3,918 ± 34	3,918 ± 34	98.0 ± 1.3
110803-2B-441	0.1307	215.04 ± 0.28	70.2 ± 3.6	98.4 ± 1.8	0.04329 ± 0.00020	2188 ± 111	4,383 ± 22	4,375 ± 22	99.6 ± 1.8
110803-2B-500	0.1024	241.17 ± 0.29	529.8 ± 4.7	95.2 ± 1.7	0.07201 ± 0.00057	541.2 ± 6.4	7,420 ± 62	7,367 ± 67	97.2 ± 1.7
110803-2B-524	0.1352	255.53 ± 0.36	85.2 ± 3.4	97.0 ± 2.0	0.05094 ± 0.00029	2522 ± 103	5,189 ± 31	5,181 ± 32	98.5 ± 2.0
110803-2B-544	0.1268	246.16 ± 0.20	85.0 ± 3.7	94.2 ± 1.3	0.05520 ± 0.00030	2640 ± 115	5,649 ± 32	5,640 ± 32	95.7 ± 1.4

Sample ID	Weight g	^{238}U ppb ^d	^{232}Th ppt	$\delta^{234}\text{U}$ measured ^e	$[\text{}^{230}\text{Th}/\text{}^{238}\text{U}]$ activity ^c	$[\text{}^{230}\text{Th}/\text{}^{232}\text{Th}]$ ppm ^d	Age uncorrected	Age corrected ^{c,e}	$\delta^{234}\text{U}_{\text{initial}}$ corrected ^b
110803-2B-550	0.1310	269.82 ± 0.40	30.2 ± 3.5	91.3 ± 2.0	0.11274 ± 0.00043	16610 ± 1947	11,890 ± 54	11,887 ± 54	94.4 ± 2.1
110803-2B-551.5	0.0934	199.51 ± 0.45	1073.7 ± 5.4	103.9 ± 3.2	0.2101 ± 0.0013	644.8 ± 5.0	22,986 ± 177	22,857 ± 188	110.8 ± 3.4
110803-2B-566.5	0.0948	309.97 ± 0.56	46.1 ± 4.9	88.4 ± 2.1	0.12240 ± 0.00054	13563 ± 1443	12,989 ± 67	12,985 ± 67	91.7 ± 2.2
110803-2B-583.5	0.0984	302.21 ± 0.47	128.4 ± 4.7	86.6 ± 2.2	0.12227 ± 0.00047	4753 ± 176	13,014 ± 60	13,004 ± 61	89.9 ± 2.3
110803-2B-610	0.0998	273.09 ± 0.45	29.4 ± 4.7	85.1 ± 1.9	0.12423 ± 0.00062	19029 ± 3014	13,237 ± 74	13,235 ± 74	88.4 ± 2.0
110803-2B-630	0.0734	298.13 ± 0.39	17.5 ± 6.3	84.1 ± 1.9	0.12491 ± 0.00052	35115 ± 12699	13,329 ± 64	13,328 ± 64	87.3 ± 2.0
110803-2B-650	0.0732	294.95 ± 0.55	484.7 ± 6.4	88.6 ± 2.7	0.13700 ± 0.00052	1377 ± 19	14,661 ± 71	14,621 ± 74	92.3 ± 2.8
110803-2B-670	0.0467	317.84 ± 0.54	333 ± 10	92.3 ± 3.0	0.13448 ± 0.00058	2119 ± 64	14,321 ± 79	14,295 ± 80	96.1 ± 3.1
110803-2B-673.5	0.0595	270.12 ± 0.97	154.5 ± 7.8	89.4 ± 5.1	0.13051 ± 0.00073	3767 ± 191	13,911 ± 110	13,897 ± 110	93.0 ± 5.3

Analytical errors are 2σ of the mean.

$${}^a[\text{}^{238}\text{U}] = [{}^{235}\text{U}] \times 137.818 (\pm 0.65\%) \text{ (Hiess et al., 2012); } \delta^{234}\text{U} = ([{}^{234}\text{U}/\text{}^{238}\text{U}]_{\text{activity}} - 1) \times 1000.$$

^b $\delta^{234}\text{U}_{\text{initial}}$ corrected was calculated based on ^{230}Th age (T), i.e., $\delta^{234}\text{U}_{\text{initial}} = \delta^{234}\text{U}_{\text{measured}} X e^{\lambda_{234}T}$, and T is corrected age.

$${}^c[\text{}^{230}\text{Th}/\text{}^{238}\text{U}]_{\text{activity}} = 1 - e^{-\lambda_{230}T} + (\delta^{234}\text{U}_{\text{measured}}/1000)[\lambda_{230}/(\lambda_{230} - \lambda_{234})](1 - e^{-(\lambda_{230} - \lambda_{234})T}), \text{ where } T \text{ is the age.}$$

Decay constants are 9.1705 x 10⁻⁶ yr⁻¹ for ²³⁰Th, 2.8221 x 10⁻⁶ yr⁻¹ for ²³⁴U (Cheng et al, 2012), and 1.55125 x 10⁻¹⁰ yr⁻¹ for ²³⁸U (Jaffey et al., 1971).

^dThe degree of detrital ^{230}Th contamination is indicated by the $[\text{}^{230}\text{Th}/\text{}^{232}\text{Th}]$ atomic ratio instead of the activity ratio.

^eAge corrections for samples were calculated using an estimated atomic $^{230}\text{Th}/\text{}^{232}\text{Th}$ ratio of 4 ± 2 ppm

Those are the values for a material at secular equilibrium, with the crustal $^{232}\text{Th}/\text{}^{238}\text{U}$ value of 3.8. The errors are arbitrarily assumed to be 50%.

Appendix (II) $\delta^{18}\text{O}$ records



MC110803-1					
Depth (mm)	Age (yr BP)	$\delta^{18}\text{O}$ (‰VPDB)	Depth (mm)	Age (yr BP)	$\delta^{18}\text{O}$ (‰VPDB)
0	354	-5.38	125	689	-5.70
3	357	-5.62	128	701	-5.20
5	360	-5.44	130	709	-5.47
8	363	-6.20	133	721	-5.54
10	365	-5.94	135	729	-5.74
13	368	-5.94	138	740	-5.92
15	371	-5.45	140	748	-5.67
18	374	-6.04	143	760	-4.75
20	376	-5.61	145	768	-5.62
23	379	-6.18	148	780	-5.39
25	382	-5.72	150	788	-5.10
28	385	-5.86	153	865	-5.15
30	387	-4.98	155	938	-5.10
33	390	-5.66	158	1047	-4.84
35	393	-5.59	160	1119	-5.56
38	396	-5.44	163	1229	-6.07
40	398	-5.33	165	1301	-5.69
43	401	-5.65	168	1379	-5.55
45	404	-5.49	170	1388	-5.94
48	407	-5.95	173	1402	-5.61
50	409	-5.75	175	1411	-5.51
53	412	-5.57	178	1425	-5.09
55	415	-5.16	180	1434	-5.27
58	418	-5.88	183	1448	-5.04
60	420	-5.11	185	1458	-5.10
63	423	-5.98	188	1472	-5.81
65	426	-5.28	190	1481	-5.14
68	429	-5.92	193	1495	-4.74
70	431	-6.45	195	1504	-5.03
73	434	-5.55	198	1518	-5.01
75	437	-6.22	200	1527	-5.71
78	440	-5.80	203	1541	-5.74
80	442	-5.54	205	1551	-5.51
83	455	-5.51	208	1564	-5.34
85	464	-5.58	210	1574	-5.40
88	477	-5.89	213	1588	-5.46
90	486	-6.03	215	1597	-5.48
93	499	-5.30	218	1611	-5.50
95	508	-5.52	220	1620	-5.65
98	521	-5.65	223	1634	-5.56
100	530	-5.73	225	1643	-5.81
103	543	-6.00	228	1657	-5.24
105	552	-5.91	230	1667	-5.43
108	565	-5.74	233	1681	-6.29
110	574	-5.71	235	1690	-5.86
113	587	-6.50	238	1704	-5.45
115	596	-5.67	240	1713	-5.54
118	619	-5.23	243	1727	-5.32
120	648	-5.36	245	1736	-5.27
123	681	-6.86	248	1750	-5.11



MC110803-1

Depth (mm)	Age (yr BP)	$\delta^{18}\text{O}$ (‰VPDB)	Depth (mm)	Age (yr BP)	$\delta^{18}\text{O}$ (‰VPDB)
250	1760	-5.25	375	2831	-6.19
253	1774	-5.25	378	2849	-5.63
255	1783	-5.51	380	2861	-6.06
258	1797	-5.01	383	2879	-6.57
260	1806	-5.46	385	2892	-6.07
263	1820	-5.40	388	2910	-6.36
265	1829	-5.51	390	2922	-5.96
268	1843	-4.92	393	2941	-5.41
270	1853	-5.19	395	2953	-5.71
273	1866	-5.60	398	2971	-5.66
275	1876	-5.14	400	2983	-5.91
278	1890	-5.08	403	3002	-5.91
280	1899	-5.27	405	3014	-5.78
283	1913	-4.92	408	3032	-5.73
285	1922	-5.15	410	3045	-5.14
288	1936	-5.47	413	3063	-5.14
290	1945	-5.61	415	3075	-5.29
293	1959	-5.73	418	3094	-5.27
295	1969	-5.44	420	3106	-4.92
298	1983	-4.95	423	3124	-5.10
300	1992	-4.98	425	3136	-4.67
303	2006	-5.64	428	3155	-4.72
305	2015	-5.72	430	3167	-5.24
308	2029	-5.75	433	3185	-4.99
310	2038	-5.93	435	3198	-5.16
313	2052	-5.94	438	3216	-4.98
315	2062	-6.00	440	3228	-5.24
318	2076	-5.75	443	3246	-6.29
320	2085	-5.81	445	3259	-5.06
323	2099	-5.44	448	3280	-5.02
325	2108	-6.07	450	3302	-5.29
328	2138	-4.59	453	3336	-5.96
330	2170	-5.21	455	3359	-5.27
333	2217	-5.53	458	3392	-4.82
335	2248	-5.70	460	3415	-5.35
338	2295	-4.27	463	3449	-5.59
340	2326	-4.53	465	3471	-5.01
343	2373	-4.42	468	3505	-4.40
345	2404	-5.56	470	3528	-5.43
348	2451	-6.26	473	3562	-5.07
350	2482	-4.79	475	3584	-5.43
353	2529	-4.91	478	3618	-4.85
355	2561	-6.18	480	3640	-5.14
358	2608	-5.07	483	3674	-5.65
360	2639	-5.93	485	3697	-5.36
363	2686	-6.02	488	3731	-5.21
365	2717	-6.36	490	3753	-5.21
368	2764	-5.85	493	3787	-4.91
370	2795	-5.34	495	3810	-5.87
373	2818	-5.65	498	3843	-5.49



MC110803-1

Depth (mm)	Age (yr BP)	$\delta^{18}\text{O}$ (‰VPDB)	Depth (mm)	Age (yr BP)	$\delta^{18}\text{O}$ (‰VPDB)
500	3866	-6.06	625	5276	-4.52
503	3900	-5.02	628	5309	-4.47
505	3922	-5.57	630	5332	-4.14
508	3956	-5.32	633	5366	-4.59
510	3979	-6.01	635	5388	-4.23
513	4013	-5.65	638	14516	-3.15
515	4035	-5.54	640	14543	-3.79
518	4069	-5.39	642	14570	-4.22
520	4092	-5.45	643	14584	-3.72
523	4125	-4.79	645	14611	-3.24
525	4148	-5.66	647	14639	-3.67
528	4182	-5.43	648	14652	-3.11
530	4204	-4.93	650	14680	-2.98
533	4238	-4.67	652	14707	-3.42
535	4261	-5.53	653	14720	-3.40
538	4295	-5.62	655	14748	-3.22
540	4317	-5.78	657	14775	-3.14
543	4351	-5.54	658	14789	-3.11
545	4373	-6.13	660	14816	-3.23
548	4407	-5.01	662	14843	-3.11
550	4430	-5.48	663	14857	-3.62
553	4464	-5.46	665	14884	-2.47
555	4486	-5.73	667	14911	-3.49
558	4520	-5.09	668	14925	-3.38
560	4543	-5.84	670	14952	-3.53
563	4576	-5.58	672	14980	-2.97
565	4599	-5.79	673	14993	-3.10
568	4633	-5.01	675	15021	-2.31
570	4655	-5.43	677	15048	-3.84
573	4689	-5.96	680	15089	-2.77
575	4712	-5.17	685	15157	-3.15
578	4746	-5.27	687	15184	-2.99
580	4768	-5.17	688	15198	-3.19
583	4802	-5.06	690	15225	-3.35
585	4825	-5.27	692	15253	-3.28
588	4858	-5.44	693	15266	-3.78
590	4881	-5.53	695	15294	-3.96
593	4915	-4.99	697	15321	-3.60
595	4937	-5.58	698	15334	-4.06
598	4971	-6.04	700	15362	-3.44
600	4994	-5.35	702	15389	-3.50
603	5028	-4.78	703	15403	-3.53
605	5050	-6.36	705	15430	-3.69
608	5084	-4.98	707	15457	-3.67
610	5106	-5.26	708	15471	-3.39
613	5140	-4.89	710	15498	-3.77
615	5163	-5.25	712	15525	-3.89
618	5197	-5.21	713	15539	-3.89
620	5219	-5.18	715	15566	-3.69
623	5253	-4.44	717	15594	-3.84



MC110803-1			MC110803-2		
Depth (mm)	Age (yr BP)	$\delta^{18}\text{O}$ (‰VPDB)	Depth (mm)	Age (yr BP)	$\delta^{18}\text{O}$ (‰VPDB)
718	15607	-3.47	0	806	-4.96
720	15635	-3.48	2	820	-5.50
722	15662	-3.59	3	827	-4.16
723	15676	-3.49	5	840	-4.33
725	15703	-3.34	7	854	-5.07
728	15744	-3.30	8	860	-5.12
730	15771	-3.37	10	874	-5.69
733	15812	-3.23	12	888	-4.97
735	15839	-3.62	13	894	-5.38
738	15880	-3.56	15	908	-5.67
740	15907	-3.85	17	921	-4.65
743	15948	-3.78	18	928	-5.90
745	15976	-3.59	20	942	-5.53
748	16017	-3.46	22	955	-4.65
750	16044	-2.90	23	962	-5.01
753	16085	-3.14	25	976	-5.19
755	16112	-3.66	27	989	-5.06
758	16153	-3.48	28	996	-5.25
760	16180	-2.94	30	1010	-5.26
763	16221	-2.98	33	1030	-5.06
765	16249	-3.05	35	1044	-5.24
768	16289	-3.25	37	1057	-5.26
770	16317	-3.10	38	1064	-4.97
773	16358	-3.53	40	1077	-5.07
775	16385	-3.43	42	1091	-4.63
778	16426	-3.10	43	1098	-5.03
780	16453	-4.26	45	1111	-5.24
783	16494	-3.57	47	1125	-5.26
785	16521	-4.09	48	1132	-5.35
788	16562	-3.67	50	1145	-5.52
790	16590	-4.43	52	1159	-4.73
793	16631	-3.36	53	1166	-5.61
			55	1179	-6.86
			57	1193	-5.07
			58	1199	-5.12
			60	1213	-6.76
			62	1227	-4.87
			63	1233	-5.39
			65	1247	-6.09
			67	1260	-5.24
			68	1267	-5.19
			70	1281	-5.38
			72	1294	-5.40
			73	1301	-5.81
			75	1315	-5.82
			77	1328	-5.26
			78	1335	-5.35
			80	1349	-5.34
			82	1362	-5.20
			83	1369	-5.16



MC110803-2

Depth (mm)	Age (yr BP)	$\delta^{18}\text{O}$ (‰VPDB)	Depth (mm)	Age (yr BP)	$\delta^{18}\text{O}$ (‰VPDB)
85	1383	-5.11	168	1969	-4.71
87	1396	-5.00	170	1987	-5.17
88	1403	-5.14	172	2000	-4.96
90	1416	-5.27	173	2008	-5.27
92	1430	-5.36	175	2025	-4.31
93	1437	-4.98	177	2039	-4.82
95	1450	-5.34	178	2047	-4.80
97	1464	-4.83	180	2062	-5.49
98	1471	-4.74	182	2083	-5.48
100	1484	-5.39	183	2093	-5.45
102	1498	-5.05	185	2114	-5.27
103	1505	-5.46	187	2135	-4.99
105	1518	-5.25	188	2145	-5.09
107	1532	-4.50	190	2166	-4.54
108	1538	-5.12	192	2187	-5.10
110	1552	-5.34	193	2197	-5.28
112	1566	-5.19	195	2218	-5.58
113	1572	-5.30	197	2239	-5.36
115	1586	-5.23	198	2250	-5.12
117	1599	-5.45	200	2270	-4.62
118	1606	-5.13	202	2291	-4.40
120	1620	-5.36	203	2302	-4.66
122	1633	-5.03	205	2322	-4.70
123	1640	-5.02	207	2343	-4.64
125	1654	-5.13	208	2354	-5.71
127	1667	-5.02	210	2375	-5.40
128	1674	-4.90	212	2395	-5.58
130	1688	-4.99	213	2406	-5.46
132	1701	-5.25	215	2427	-5.22
133	1708	-5.33	217	2447	-4.81
135	1722	-5.33	218	2458	-5.49
137	1735	-5.09	220	2479	-5.46
138	1742	-5.54	222	2500	-5.59
140	1755	-5.33	223	2510	-5.94
142	1769	-4.99	225	2531	-5.75
143	1777	-5.21	227	2552	-5.23
145	1794	-5.45	228	2562	-5.74
147	1808	-5.36	230	2583	-5.42
148	1815	-5.22	233	2614	-5.75
150	1833	-5.25	235	2635	-5.36
152	1846	-5.69	237	2656	-5.67
153	1854	-5.72	238	2666	-5.75
155	1871	-5.90	240	2687	-5.15
157	1885	-5.79	242	2699	-4.78
158	1892	-5.71	243	2705	-5.39
160	1910	-5.51	245	2717	-5.91
162	1923	-5.42	247	2728	-5.60
163	1931	-5.50	248	2734	-6.55
165	1948	-5.31	250	2746	-5.27
167	1962	-5.09	252	2758	-5.53



MC110803-2

Depth (mm)	Age (yr BP)	$\delta^{18}\text{O}$ (‰VPDB)	Depth (mm)	Age (yr BP)	$\delta^{18}\text{O}$ (‰VPDB)
253	2764	-5.73	340	3277	-5.00
255	2776	-5.29	342	3289	-5.44
257	2787	-4.76	343	3295	-5.14
258	2793	-5.37	345	3307	-5.41
260	2805	-4.96	347	3319	-5.20
262	2817	-5.01	348	3325	-5.26
263	2823	-5.46	350	3336	-5.33
265	2835	-5.14	352	3348	-5.24
267	2846	-5.27	353	3354	-5.62
268	2852	-5.14	355	3366	-5.41
270	2864	-5.28	357	3378	-4.81
272	2876	-5.49	358	3384	-5.01
273	2882	-6.32	360	3395	-4.93
275	2894	-5.51	362	3407	-4.91
277	2905	-5.26	363	3413	-5.16
278	2911	-5.40	365	3425	-5.10
280	2923	-5.50	367	3445	-5.35
282	2935	-5.28	368	3455	-4.92
283	2941	-5.53	370	3474	-5.13
285	2953	-5.25	372	3494	-4.94
287	2964	-4.66	373	3504	-4.89
288	2970	-4.92	375	3524	-5.00
290	2982	-4.48	377	3543	-5.03
292	2994	-4.79	378	3553	-4.73
293	3000	-5.25	380	3573	-4.91
295	3012	-4.56	382	3593	-5.11
298	3029	-5.55	383	3602	-5.45
300	3041	-4.88	385	3622	-5.27
302	3053	-4.99	387	3642	-5.23
303	3059	-4.64	388	3652	-4.70
305	3071	-4.47	390	3672	-4.86
308	3088	-5.37	392	3691	-5.17
310	3100	-4.72	393	3701	-4.80
312	3112	-4.90	395	3721	-5.02
313	3118	-5.50	397	3741	-5.42
315	3130	-4.82	398	3750	-4.80
317	3142	-5.83	400	3770	-4.22
318	3148	-5.47	402	3790	-5.05
320	3159	-5.55	403	3800	-4.92
322	3171	-5.06	405	3819	-5.17
323	3177	-5.09	407	3839	-5.55
325	3189	-5.16	408	3849	-5.33
327	3201	-5.04	410	3869	-4.54
328	3207	-6.61	412	3888	-5.01
330	3218	-5.01	413	3898	-4.97
332	3230	-5.24	415	3918	-5.01
333	3236	-4.90	417	3954	-5.74
335	3248	-4.79	418	3972	-5.45
337	3260	-5.22	420	4007	-5.58
338	3266	-5.53	422	4043	-5.63



MC110803-2

Depth (mm)	Age (yr BP)	$\delta^{18}\text{O}$ (‰VPDB)	Depth (mm)	Age (yr BP)	$\delta^{18}\text{O}$ (‰VPDB)
423	4061	-4.20	508	5027	-5.14
425	4097	-4.87	510	5046	-5.36
427	4133	-5.35	512	5066	-5.33
428	4151	-4.98	513	5075	-5.69
430	4186	-4.94	515	5094	-5.82
432	4222	-4.95	517	5114	-5.87
433	4240	-4.86	518	5123	-5.86
435	4276	-4.76	520	5143	-5.30
437	4311	-5.02	522	5162	-5.37
438	4329	-4.48	523	5171	-5.07
440	4365	-5.18	525	5204	-4.86
442	4393	-4.79	527	5250	-4.78
443	4402	-5.19	528	5273	-4.56
445	4421	-5.13	530	5319	-4.55
447	4441	-5.25	531	5342	-4.66
450	4470	-4.96	532	5365	-4.88
452	4489	-5.67	533	5388	-3.71
453	4498	-5.10	534	5411	-5.36
455	4518	-5.08	535	5433	-5.37
457	4537	-5.09	536	5456	-3.98
458	4546	-4.71	537	5479	-3.55
460	4566	-5.34	538	5502	-3.69
462	4585	-5.08	539	5525	-3.91
463	4595	-5.35	540	5548	-3.72
465	4614	-5.23	541	5571	-3.65
467	4633	-5.25	542	5594	-3.99
468	4643	-5.04	543	5617	-3.95
470	4662	-5.04	544	5640	-3.93
472	4681	-5.11	550	11887	-3.81
473	4691	-4.82	551	11920	-3.83
475	4710	-5.13	552	11954	-3.25
477	4729	-5.56	554	12020	-2.91
478	4739	-5.23	555	12054	-2.68
480	4758	-5.70	556	12087	-2.77
482	4777	-5.08	557	12120	-2.63
483	4787	-5.42	558	12154	-4.15
485	4806	-5.47	559	12187	-3.21
487	4825	-5.42	560	12220	-3.50
488	4835	-5.63	561	12254	-3.61
490	4854	-5.72	562	12287	-3.80
492	4873	-5.43	563	12320	-3.68
493	4883	-5.43	564	12354	-4.32
495	4902	-5.19	565	12387	-4.26
497	4921	-5.62	566	12420	-3.64
498	4931	-5.53	567	12454	-3.90
500	4950	-5.39	568	12487	-3.24
502	4969	-5.35	569	12521	-4.03
503	4979	-4.87	570	12554	-4.22
505	4998	-5.33	571	12587	-3.36
507	5018	-5.45	572	12621	-3.18



MC110803-2					
Depth (mm)	Age (yr BP)	$\delta^{18}\text{O}$ (‰VPDB)	Depth (mm)	Age (yr BP)	$\delta^{18}\text{O}$ (‰VPDB)
573	12654	-3.45	625	14013	-3.56
574	12687	-3.43	626	14037	-3.60
575	12721	-3.51	627	14062	-3.59
576	12754	-3.27	628	14086	-3.49
577	12787	-3.53	629	14110	-3.52
578	12821	-3.54	630	14135	-3.51
579	12854	-3.42	631	14159	-3.56
580	12887	-3.36	632	14183	-3.71
581	12921	-3.85	633	14208	-2.65
582	12954	-3.70	634	14232	-3.49
583	12987	-3.73	635	14256	-3.32
584	13016	-3.59	636	14281	-3.52
585	13040	-3.72	637	14305	-3.56
586	13065	-3.74	638	14329	-3.35
588	13113	-3.43	639	14354	-3.50
589	13138	-4.84	640	14378	-3.43
590	13162	-3.39	641	14402	-3.55
591	13186	-3.73	642	14426	-3.46
592	13211	-3.83	643	14451	-3.28
593	13235	-4.21	644	14475	-4.03
594	13259	-3.51	645	14499	-3.45
595	13284	-3.63	646	14524	-3.56
596	13308	-3.60	647	14548	-3.83
597	13332	-3.56	648	14572	-3.25
598	13357	-3.92	649	14597	-3.58
599	13381	-4.13	650	14621	-3.52
600	13405	-3.92	651	14645	-3.22
601	13430	-3.74	652	14670	-3.25
602	13454	-4.22	653	14694	-3.56
603	13478	-3.30	654	14718	-3.43
604	13502	-3.62	655	14743	-2.79
605	13527	-3.32	656	14767	-4.01
606	13551	-3.69	657	14791	-4.03
607	13575	-3.78	658	14816	-2.50
608	13600	-3.66	659	14840	-2.35
609	13624	-4.00	660	14864	-2.78
610	13648	-3.85	661	14888	-2.37
611	13673	-3.90	662	14913	-2.74
612	13697	-4.03	663	14937	-4.44
613	13721	-3.32	664	14961	-2.88
614	13746	-3.21	665	14986	-2.54
615	13770	-3.67	666	15010	-2.57
617	13819	-3.47	667	15034	-2.53
618	13843	-3.78	668	15059	-4.02
619	13867	-3.61	669	15083	-2.62
620	13892	-3.67	670	15107	-2.74
621	13916	-3.59			
622	13940	-3.66			
623	13964	-3.33			
624	13989	-3.64			



090721-2MC

Depth (mm)	Age (yr BP)	$\delta^{18}\text{O}$ (‰VPDB)	Depth (mm)	Age (yr BP)	$\delta^{18}\text{O}$ (‰VPDB)
0	11547	-3.86	50	12636	-3.84
1	11571	-4.03	51	12656	-2.84
2	11594	-4.20	52	12664	-3.53
3	11618	-3.97	53	12678	-3.57
4	11642	-3.90	54	12696	-3.31
5	11666	-3.94	55	12706	-3.53
6	11691	-3.97	56	12720	-2.84
7	11713	-4.24	57	12736	-2.98
8	11737	-3.51	58	12748	-3.09
9	11764	-3.25	59	12762	-3.37
10	11784	-3.76	60	12776	-3.16
11	11808	-3.62	61	12811	-3.37
12	11838	-4.01	62	12846	-3.77
13	11855	-3.73	63	12880	-3.43
14	11879	-3.93	64	12915	-2.96
15	11911	-3.93	65	12950	-2.45
16	11927	-3.89	66	12985	-3.53
17	11950	-3.52	67	13020	-3.91
18	11984	-3.52	68	13055	-2.98
19	11998	-3.84	69	13089	-3.24
20	12021	-4.13	70	13124	-3.25
21	12057	-4.13	71	13159	-3.19
22	12069	-4.00	72	13194	-2.76
23	12093	-4.05	73	13229	-2.88
24	12130	-4.07	74	13263	-2.98
25	12140	-3.79	75	13298	-3.31
26	12164	-4.02	76	13333	-3.74
27	12203	-4.07	77	13368	-3.47
28	12211	-4.10	78	13403	-2.96
29	12235	-4.04	79	13438	-3.09
30	12277	-3.85	80	13472	-2.97
31	12282	-3.86	81	13507	-2.96
32	12306	-3.80	82	13542	-3.03
33	12350	-3.70	83	13577	-3.27
34	12354	-3.76	84	13612	-2.93
35	12377	-3.90	85	13646	-3.30
36	12423	-4.13	86	13681	-3.04
37	12425	-4.21	87	13716	-2.79
38	12449	-3.80	88	13751	-3.13
39	12496	-3.52	89	13786	-3.02
40	12496	-3.54	90	13821	-2.71
41	12510	-3.61			
42	12536	-3.10			
43	12538	-3.42			
44	12552	-3.71			
45	12576	-3.32			
46	12580	-3.08			
47	12594	-3.30			
48	12616	-3.63			
49	12622	-3.56			